Development of a methodology based on deep learning to design compressive seismic acquisition geometries.

María Alejandra Hernández Rojas

Master thesis to qualify for the title of Master of Science in Geophysics

Advisor

Henry Arguello Fuentes

PhD. in Electrical and Computer Engineering

Co-advisor

Yesid Paul Goyes Peñafiel

PhD(c). in Computer Sciences

Universidad Industrial de Santander

Faculty of Sciences

Department of Physics

Bucaramanga

2023

Dedicatory

To my parents for being my unconditional support

and friends for making my life funny.

Acknowledgments

This thesis was supported by the project 110287780575 through the agreement 785-2019 between the *Agencia Nacional de Hidrocarburos* and the *Ministerio de Ciencia, Tecnología e Innovación* and *Fondo Nacional de Financiamiento para la Ciencia, la Tecnología y la Innovación Francisco José de Caldas.*

To my advisor for his support and assistance during the last two years. Also, for the academic and personal advice that helped shape me into the professional I am.

Once again, to my co-advisor Paul Goyes, who has been involved in my academic training during the last five years.

To people in HDSP group for their support and criticism of my works. Especially to Laura Galvis and Claudia Correa for their reviewer and valuable contribution to this work.

To Ivan Ortiz and Brayan Monroy for their friendship during this stage of my life.

Table of Contents

List of Figures

List of Tables

Abstract

Title: Development of a methodology based on Deep Learning for the design of compressive seismic acquisition geometries. *

Autor: María Alejandra Hernández Rojas **

Keywords: Seismic Geometry, End-to-End Optimization, Seismic Data Reconstruction, Sensing Pattern, Undersampling Rate.

Description: Seismic acquisition is necessary to explore the subsurface for discovering new hydrocarbon targets. High-quality seismic images require a high-resolution regular-spaced acquisition. Still, the high costs and environmental impacts have led to the development of seismic surveys with fewer sources and receivers. However, using random, jittered, or uniform sensing schemes, the current selection of removed data leads to suboptimal seismic image quality recovery. A guided design of undersampled seismic surveys is crucial in determining the quality of the reconstructed information. To address this issue, this work proposes an end-to-end optimization to design an undersampled seismic acquisition that preserves the quality of the reconstructed data. The sensing pattern is modeled as a deep binary layer to learn the optimal location of receivers and sources for a particular seismic survey. A deep neural network recovers the underlying removed data. Once the optimal sensing pattern is designed, it can be used as a seismic geometry in an area with a similar geological setting to the training data set. The proposed methodology was compared with random, jittered, and uniform sensing schemes through experiments on synthetic and real seismic data sets. The results demonstrate that a guided design improves the quality of the reconstructed data by up to 4 dB.

---

* Master Thesis

** Faculty of Sciences. Department of Physics. Advisor: Henry Arguello Fuentes, PhD. in Electrical and Computer Engineering.

Resumen

Título: Desarrollo de una metodología basada en Aprendizaje Profundo para el diseño de geometrías de adquisición sísmica compresiva. [*]

Autor: María Alejandra Hernández Rojas [**]

Palabras Clave: Geometría Sísmica, Optimización de Extremo a Extremo, Reconstrucción de Datos Sísmicos, Patrón de Submuestreo, Tasa de Submuestreo.

Descripción: La adquisición sísmica es esencial para encontrar nuevos yacimientos de hidrocarburos. Para adquirir imágenes sísmicas de alta calidad, se requiere una adquisición densa espaciada regularmente. Sin embargo, los altos costos de adquisición y los impactos ambientales, han conducido a diseñar levantamientos sísmicos con menos fuentes y receptores. Actualmente, los esquemas de submuestreo tradicionales son: aleatorio, *jittered* y uniforme, los cuales conducen a una recuperación subóptima de la imagen sísmica. Por lo tanto, este trabajo propone una optimización de extremo a extremo para diseñar una adquisición sísmica submuestreada que permita obtener información reconstruida de alta calidad. El patrón de muestreo se modela como una capa binaria profunda para conocer la ubicación óptima de receptores y fuentes, al tiempo que una red neuronal recupera los datos eliminados. Después de diseñar el patrón de muestreo, se puede utilizar como geometría sísmica en un área geológicamente similar al conjunto de datos de entrenamiento. La metodología propuesta se comparó con los esquemas de muestreo tradicionales mediante experimentos con datos sísmicos sintéticos y reales. Los resultados demuestran que un diseño aprendido mejora la calidad de los datos reconstruidos en hasta 4 dB.

---

[*] Trabajo de grado

[**] Facultad de Ciencias. Escuela de Física. Director: Henry Arguello Fuentes, Doctorado en Ingeniería Eléctrica y Computación.

Introduction

A seismic survey uses sources and receivers to create an image of the Earth's structure at depth. The sources generate seismic waves, while the receivers record the reflected waves (Stone and Meeder, 1994). To recover the analog signal accurately, the Nyquist-Shannon sampling theorem requires that the signal be sampled at least twice its maximum frequency in both time and spatial domains (Shannon, 1949). Therefore, seismic surveys are designed to adhere to this theorem.

For land and marine 2D surveys, the sources and receivers are arranged linearly and in parallel. In 3D surveys, swath and parallel swath designs are used, with orthogonal and parallel source and receiver lines, respectively (Evans, 1997; Stone and Meeder, 1994). However, cost and environmental regulations may cause irregular and incomplete surveys, leading to a lack of information and lower-quality seismic data (Chaouch and Mari, 2006).

Therefore, the challenge is to design a seismic survey that acquires high-quality images while being cost-effective, time-efficient, and environmentally conscious. However, the current steps in designing a seismic survey, such as the sensing matrix and data reconstruction, do not consider the optimal placement of sources and receivers for the highest quality of the subsequent reconstructed seismic data.

Similarly, there is a research topic in spectral imaging related to the acquisition of compressive measurements. The idea is to design binary coding patterns to strategically sense a scene with fewer samples than conventional sensing schemes (Hinojosa et al., 2018;

Bacca et al., 2021; Jacome et al., 2022). Therefore, inspired by the binary-coded aperture design, this work exploits an end-to-end (E2E) methodology to learn the optimal location of receivers and sources for a specific seismic survey. The goal is to ensure high-quality reconstruction of the non-acquired seismic data. To accomplish this, an existing seismic data set with a similar geological setting to the target area is used to train the model. During training, a binary sensing layer designs an optimal seismic acquisition pattern for obtaining undersampled data. Simultaneously, a U-Net convolutional neural network reconstructs the removed information. Finally, the trainable parameters of the sensing layer and the U-Net are updated jointly to minimize the error between the reconstructed and ground truth data. As a result, the sources and receivers with a higher probability of being removed by the sensing pattern have a lower reconstruction error in the optimization framework.

Contributions of the thesis

The main contributions of the thesis are:

- A E2E methodology for compressive seismic survey design was developed by jointly optimizing a binary training layer representing the sensing pattern and a reconstruction network to recover the missing information.

- This work successfully achieved low reconstruction error of seismic data by strategically selecting the optimal location of removed receivers and sources in an E2E methodology. Specifically, the sensing pattern is designed for a particular seismic survey and can be applied to an area with a similar geological setting as the training data set.

- The proposed method uses a trainable binary sensing layer to design the optimal sensing pattern for any seismic acquisition geometry. Furthermore, this layer is adaptable and can be combined with any existing neural network architecture to enhance the recovery task further.

- The effectiveness and efficiency of the proposed E2E model are demonstrated on different data sets in this work. The model outperforms traditional sensing schemes and achieves better reconstruction results.

Publications associated with the thesis

The challenges faced and solved during the development of this thesis served as an opportunity to publish a journal paper and different conference papers:

Journal papers:

1. Hernandez-Rojas, A., & Arguello, H. Design of Undersampled Seismic Acquisition Geometries Via End-to-End Optimization. Submitted to *IEEE Transactions on Geoscience and Remote Sensing*.

Conference papers:

1. Hernandez-Rojas, A., & Arguello, H. (2022). 3D Geometry Design via End-To-End Optimization for Land Seismic Acquisition. *2022 IEEE International Conference on Image Processing (ICIP)*, 4053–4057. https://doi.org/10.1109/ICIP46576.2022.9897295

2. Bacca, J., Hernandez-Rojas, A., & Arguello, H. (2022). Deep Coding Patterns Design for Compressive Near-Infrared Spectral Classification. *2022 30th European Signal Processing Conference (EUSIPCO)*, 548–552. https://doi.org/10.23919/EUSIPCO55093.2022.9909534

3. Jacome R., Hernandez-Rojas, A., & Arguello, H. (2022). Probabilistic Regularization for End-to-End Optimization in Compressive Imaging. *Imaging and Applied Optics Congress 2022 (3D, AOA, COSI, ISA, pcAOP)*, paper CW1B.1. https://opg.optica.org/abstract.cfm?URI=COSI-2022-CW1B.1

4. Jacome R., H, Arguello., Hernandez-Rojas, A., & Goyes-Peñafiel, P. (2023). Divergence-Based Regularization for End-to-End Sensing Matrix Optimization in Compressive Sampling Systems. *SIGNAL 2023: The Eighth International Conference on Advances in Signal, Image and Video Processing*, 72–78. https://www.thinkmind.org/index.php?view=article&articleid=signal_2023_1_150_60077

1. Problem statement

Traditional land seismic surveys consist of laying geophone lines parallel to each other in the inline direction and source lines perpendicular to them in the cross-line direction, producing a uniformly spaced grid. However, the high economic costs associated with seismic surveys have generated interest in reducing the number of geophones and sources in the field. Some authors have addressed this problem by proposing random, *jittered* (Hennenfent and Herrmann, 2008), uniform compressive acquisition schemes, and subsequent recovery of the non-acquired data using iterative algorithms. However, these approaches are general for any seismic acquisition, and the selection of sources or geophones does not consider the data correlation and the importance of seismic data reconstruction. Therefore, it is crucial to develop an adequate methodology to design compressive acquisition geometries that simultaneously ensure the high resolution of the reconstructed seismic data.

1.1. Research question

Which is the methodology for designing compressive acquisition geometries that guarantee the high quality of the recovered seismic data and, in turn, allow for reducing economic costs and environmental impacts?

1.2. Hypothesis

End-to-end deep learning models for seismic data can extract characteristics from seismic signals, enabling the design of a compressive acquisition geometry to reduce economic costs and environmental impacts while guaranteeing high-quality reconstructed data.

2. Objectives

General Objective

To develop a methodology based on deep learning for designing compressive seismic acquisition geometries.

Specific Objectives

1. To mathematically formulate the acquisition model of partially observed seismic data in 2-D and 3-D acquisition geometries.

2. To develop an end-to-end deep learning-based model to jointly learn an optimized seismic acquisition design and the seismic data reconstruction.

3. To generate a synthetic seismic data set for the simulations using a 2-D and 3-D seismic acquisition.

4. To evaluate the effectiveness of the proposed method with the state-of-the-art seismic acquisition geometries and reconstruction methods using synthetic and real data sets.

3. Review of the state-of-the-art on the design of compressive seismic acquisition geometries

Designing a seismic survey with a limited number of sources and receivers poses a classic NP-Complete problem since finding the optimal solution requires evaluating all possible combinations of source and receiver locations (Manohar et al., 2018). To address this challenge, various strategies have been proposed by different authors, which can be broadly classified into three categories: model-driven methods based on geophysical parameters, model-driven methods based on data priors, and data-driven methods based on deep learning.

3.1. Model-driven methods based on geophysical parameters

Methods based on geophysical parameters involve optimizing algorithms to minimize or maximize an objective function related to specific seismic acquisition parameters, such as bin size, maximum offset, largest minimum offset, or geometry type. Notably, in Djikpesse et al. (2012), a Bayesian methodology for seismic survey design is proposed, which seeks to maximize the resolution of the acquired data. Similarly, in Monsegny (2017), the objective function aims to minimize the sum of the distances between source-receiver pairs to obtain the best possible seismic survey for illuminating a specific target. However, since multiple geophysical parameters can affect the quality of the acquired information, these methods require the optimization of multiple variables simultaneously, resulting in increased problem complexity (Monsegny, 2017).

3.2. Model-driven methods based on data priors

Approaches based on data priors use compressive sensing (CS) and low-rank techniques. The CS method assumes that the signal has a sparsity structure on a transform basis, which enables it to be recovered from a small number of samples, lower than what the Nyquist-Shannon theorem dictates (Baraniuk and Steeghs, 2017). Various undersampling schemes based on CS have been proposed (Figure 1), such as *jittered* undersampling (Hennenfent and Herrmann, 2008), piecewise random undersampling (Wang et al., 2011), Bernoulli-based random undersampling (Cai et al., 2014), and local random undersampling (Liu et al., 2015). These strategies employ a random undersampling technique by controlling the maximum gap between two adjacent acquired receivers, resulting in improved seismic wavefield reconstruction compared to purely random and uniform undersampling schemes. In Mosher et al. (2012), a Non-Uniform Optimal Sampling (NUOS) methodology was proposed using Monte Carlo simulation to select optimal source locations, and CS techniques to reconstruct non-acquired information. Another CS-based approach explores the mutual coherence between the sensing matrix and the transformation basis to select optimal sensor locations, thereby reducing aliasing and reconstruction error on seismic data in frequency-wavenumber (f-k) and time-space (t-x) domains (Titova et al., 2019; Campman et al., 2017; Jamali-Rad et al., 2016). Concerning low-rank techniques, they leverage the high correlation of the data to infer missing information from the measurements (Popa et al., 2021). In Zhang et al. (2022), a seismic survey design for receiver location was developed that minimizes the spectral ratio

Figure 1. Schematic comparison between different undersampling schemes.

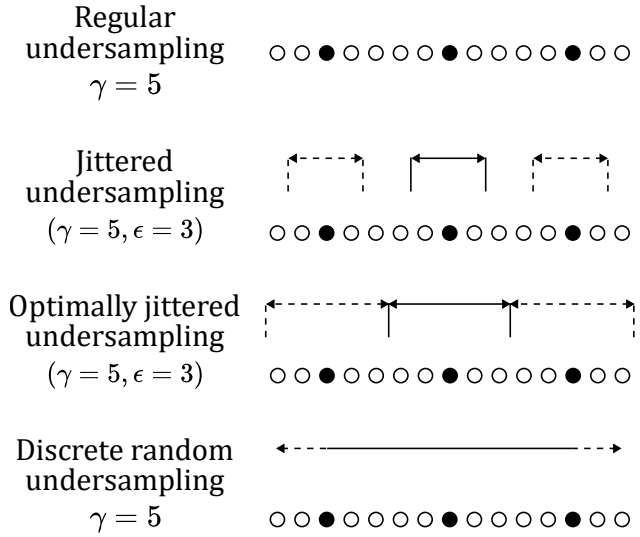

Note: The circles define the fine grid on which the original signal is alias free. The solid circles represent the actual sampling points for the different undersampling schemes. The jitter parameter ϵ relates to how far the actual jittered sampling point can be from the regular coarse grid, effectively controlling the size of the maximum acquisition gap, and γ refers to the undersampling factor (Hennenfent and Herrmann, 2008).

concerning the sensing matrix under the assumption that a transform domain exists in which the fully sampled seismic data, organized as a matrix, exhibits a low-rank structure.

Lastly, the third approach proposes methodologies that combine geophysical parameters and data priors, as presented in Bhuiyan and Sacchi (2015) and Jiang et al. (2018). These methods aim to minimize the mutual coherence while fulfilling geophysical and operational constraints related to the seismic acquisition parameters in common midpoint-offset, and common shot gather domains, respectively. However, it should be noted that model-based methods rely heavily on a deep understanding of the physical phenomenon and require mathematical modeling, which may have some limitations. Additionally, prior-based approaches such as CS assume that the data is sparse under certain transforms or low-rank, which

assumes that the data contains structural redundancies. These assumptions may not be adaptable to different types of seismic data due to variations in environmental and geological settings in which they were acquired, potentially leading to low-quality image restoration of complex structures (Yu and Ma, 2021).

3.3. Data-driven methods based on artificial intelligence

Data-driven strategies for seismic survey design have the advantage of not requiring prior assumptions to be incorporated into the solution, unlike model-driven methods that rely on mathematical modeling of the physical phenomenon. However, only a few works related to seismic survey design use this approach. In one such work (Blacquiere and Nakayama, 2019), a data-driven method using a genetic algorithm is proposed to optimize receiver acquisition design. However, the authors assume prior knowledge about the subsurface (e.g., velocity models) for modeling the ideal data via finite elements, which may not be available in frontier basins where exploration activities have yet to be carried out. In another work, Guo and Sacchi (2020), Proper Orthogonal Decomposition is used to extract a representation basis from a training data set. The optimal sensing matrix for receivers is obtained via dimensionality reduction and QR factorization. However, the reconstruction of the testing data set is carried out via the least squares method, which can become computationally expensive if the dimensions of the data increase. Therefore, data-driven approaches for seismic survey design are still in their early stages of development and require further research to apply to more complex scenarios.

Table 1 summarizes the works presented in this section for the design of compressive

seismic acquisition geometries.

Table 1
Summary of the methods for the design of compressive seismic acquisition geometries.

Method	**Assumption**	**Limitations**	**Advantages**	**SOAT**
Model-driven based on geophysical parameters	A regular-spaced and uniform seismic acquisition geometry	These methods do not consider the environmental constraints that cause seismic geometries to be incomplete and irregular	Model-based methods that do not require previous seismic data, only the acquisition geometry parameters	- Bayesian methodology to seismic survey design to maximize the resolution of the data (Djikpesse et al., 2012) - Seismic survey design to maximize the target illumination (Monsegny, 2017)
Model-driven based on data priors	The acquired signal has a sparsity structure on a transform basis or exhibits low-rank	Sparsity, and low-rank assumptions are not adaptable for all seismic data sets	Model-based methods that do not require previous seismic data	- Undersampling schemes such as jittered (Hennenfent and Herrmann, 2008) and piecewise random (Wang et al., 2011) - Seismic survey design by minimizing the spectral ratio (Zhang et al., 2022)
Data-driven based on artificial intelligence	There is minimal or no multicollinearity among the independent variables	- Requires a high amount of data to train the learning models	- Automation of processes without requiring additional human supervision - Ability to work and perform advanced analysis with unstructured data	- Genetic algorithm for receiver acquisition design (Blacquiere and Nakayama, 2019) - Dimensionality reduction and QR factorization for sensing matrix design (Guo and Sacchi, 2020)

Note: SOAT denotes the main state-of-the-art works related to compressive seismic survey design.

4. Review of the state-of-the-art on seismic data reconstruction algorithms

After designing the optimal acquisition geometry and simulating undersampled measurements to test seismic data reconstruction algorithms, the problem of missing seismic traces (receivers) or shots (sources) can be addressed through interpolation algorithms. Although interpolation methods have been extensively studied, they face mathematical challenges due to the problem of having less sampled data than the original image. This results in an inconsistent system, making the original data reconstruction problem mathematically ill-conditioned.

Two main approaches to seismic data reconstruction methods are model-driven and data-driven, which are explained below.

4.1. Model-driven methods

Several research papers have proposed traditional model-based methods to reconstruct missing seismic information. Among the recent works for the reconstruction of traces (missing receivers) and shots (missing sources), some involve compressive sensing techniques (Galvis et al., 2020; Goyes-Penafiel et al., 2021; Shu et al., 2020; Titova et al., 2021; Villarreal et al., 2019, 2018), regularizers that promote low rank (Lopez et al., 2016; Ma, 2013; Popa et al., 2021; Wu et al., 2020), and algorithms based on Projections Onto Convex Sets (POCS) (Jiang et al., 2018; Trickett et al., 2010; Wang et al., 2010). A fundamental requirement to implement model-based methods is to assume prior signal information. For instance, compressive sensing techniques assume that a specific transformation basis promotes sparsity in the data

Figure 2. Schematic representation for compressive sensing and low-rank approaches.

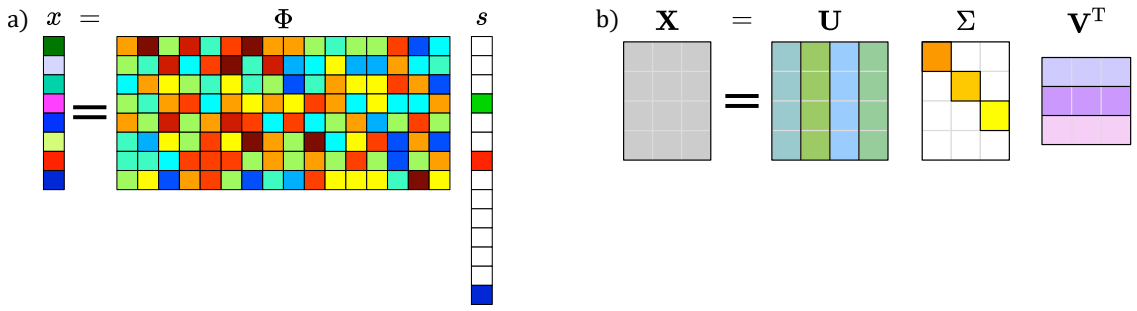

Note: a) Compressive sensing: s is a sparse representation of the signal x using a transformation basis Φ. b) Low-rank: Singular value decomposition (SVD) of the matrix $\mathbf{X}$, where $\mathbf{U}$ and $\mathbf{V}^{\mathrm{T}}$ are the orthogonal basis, and Σ is a diagonal matrix containing the singular values.

coefficients (Figure 2a), and low rank assumes that the data contains structural redundancies and high correlation (Figure 2b). However, these a priori assumptions cannot adapt to different types of seismic data because they vary depending on the geological and environmental settings in which they were acquired, leading to low-quality image reconstruction in areas with complex structures (Yu and Ma, 2021).

4.2. Data-driven methods

Traditional model-based methods like compressive sensing require certain assumptions to be built into the solution. On the other hand, Deep Learning (DL) algorithms automatically learn data's inherent structure using optimization techniques and databases (LeCun et al., 2015). As a result, DL has quickly become state-of-the-art in many fields, including Earth Sciences, where significant advances have been made in matrix completion and image reconstruction. In particular, Convolutional Neural Networks (CNNs) - composed of alternating convolutional and fully connected layers (Krizhevsky et al., 2017), see Figure 3 - have been successfully used to reconstruct seismic traces in both pre-stack (Chai et al., 2020; Liu et al.,

Figure 3. Network architecture of a convolutional autoencoder.

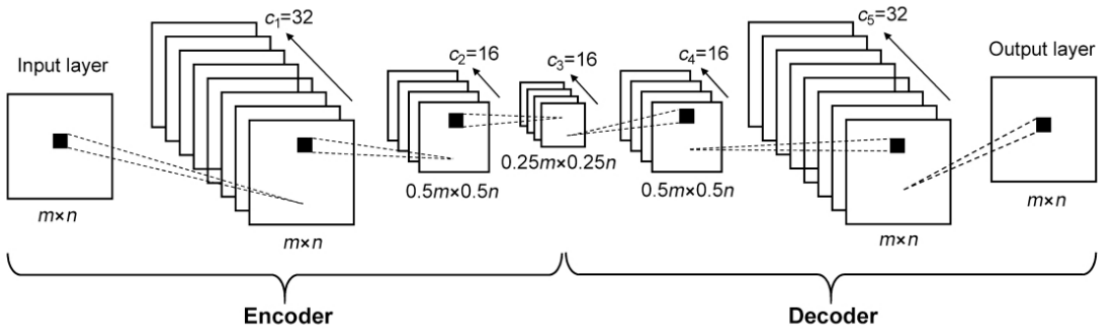

Note: After Wang et al. (2020).

2021; Wang et al., 2019, 2020) and post-stack (Chai et al., 2020; Liu et al., 2021) domains, and seismic shots (Tang et al., 2022; Wang et al., 2020) to a lesser extent. Furthermore, due to their generalized training and complete connectivity between adjacent layers, these networks are highly versatile and capable of processing signals of any dimension, such as 1-D audio, 2-D images, and 3-D videos (Alzubaidi et al., 2021; Zeiler and Fergus, 2014).

Table 2 summarizes the works presented in this section to reconstruct missing seismic data.

Table 2
Summary of the methods for reconstructing missing seismic data.

Method	**Assumption**	**Limitations**	**Advantages**	**SOAT**
Compressive Sensing	The sparsity of a signal can be leveraged through optimization to recover it from fewer samples than what is required by the Nyquist-Shannon sampling theorem	The method relies on the sparsity of the signal in certain transformation domains and also requires that the sampling points of the signal exhibit incoherence, which is achieved by applying the isometric property	Model-based method that does not require the use of large volumes of data	Seismic shot reconstruction: - From non-uniformly sampled sources (Galvis et al., 2020) - Through a curvelet transform taking into account its basis functions (Titova et al., 2021) - Using consensus equilibrium optimization strategies (Goyes-Penafiel et al., 2021)
Low-rank algorithms	This approach aims to leverage the structural redundancies and high correlations present in the data, enabling them to be represented as a linear combination of subsequent data	- The data that is acquired must exhibit a high degree of correlation among its elements - The method suffers from low computational efficiency	Model-based method that does not require the use of large volumes of data	Seismic traces reconstruction: - From a low-rank matrix recovery workflow that uses unstructured observations (Lopez et al., 2016) - Using seismic data with five spatial dimensions (Wu et al., 2020) - Using a low-rank tensor optimization algorithm (Popa et al., 2021)
Deep learning	CNNs have an explicit assumption that their inputs are images, which enables them to encode certain properties into the architecture, allowing them to recognize specific elements in images through feature extraction	- DL requires a high amount of data to train the learning models - Neural networks analyze millions of parameters, which increases their computational cost	- Automation of processes without requiring additional human supervision - Ability to work and perform advanced analysis with unstructured data	Seismic trace reconstruction: - Deep image prior approach (Liu et al., 2021) Seismic shot reconstruction: - Using the spatial reciprocity of the Green function based on Deep Learning (Wang et al., 2020) - From a residual U-Net network (Tang et al., 2022)

Note: SOAT denotes for the main state-of-the-art works related to seismic data reconstruction.

5. Mathematical formulation of seismic data acquisition

This section details the mathematical model and optimization problem of acquiring compressive seismic data.

5.1. Vector mathematical model

Mathematically, seismic data can be represented as an array $\mathbf{x} \in \mathbb{R}^{MNS}$, where $M,\ N,\ S$ are the samples in time, geophone, and shot domains, respectively. The seismic data reconstruction problem consists in recovering $\mathbf{x}$ from a vector of compressed measurements $\mathbf{y} \in \mathbb{R}^{MNS}$, where the missing seismic data are represented with zero values. In this way, the linear relationship between the data to be reconstructed and the compressed measurements is defined using the equation

$$\mathbf{y} = \mathbf{\Phi x} + \mathbf{w}, \tag{1}$$

where $\mathbf{\Phi} \in \{0,1\}^{MNS \times MNS}$ is a diagonal matrix with values of 1 for the acquired data and 0 for the missing data, and $\mathbf{w} \in \mathbb{R}^{MNS}$ is the seismic noise, which is mainly random or coherent. Random noise does not correlate either with the neighboring channels (i.e., no spatial correlation) or along the same channel (i.e., no temporal correlation). Coherent noise, however, is part of the data that correlates spatially and/or temporally Kumar and Ahmed (2011).

The optimization problem related to the seismic data reconstruction has a data fidelity

term used as a cost function that ensures that the acquired measurements coincide with the reconstructed ones, plus a regularizer term that improves the problem conditioning by introducing prior assumptions over the data.

Mathematically, the optimization problem is defined as

$$\mathbf{x}^* = \arg\min_{\mathbf{x}} \frac{1}{2}||\mathbf{y} - \mathbf{\Phi}\mathbf{x}||_2^2 + \rho\mathcal{R}(\mathbf{x}), \tag{2}$$

where the first term is the fidelity term, and the second one is a regularizer with a weighting parameter ρ. The main regularizers in the state-of-the-art are the sparsity over a transformation basis $\mathcal{R}(\mathbf{x}) = ||\Psi\mathbf{x}||_1$ and low-rank over a lineal transformation domain $\mathcal{R}(\mathbf{x}) = ||\mathcal{T}(\mathbf{x})||_*$, as described by Chen et al. (2016).

5.2. Tensor mathematical model

The cross-spread is a fundamental acquisition geometry that involves a single source line and one perpendicular receiver line. If the source line is extended to cover multiple perpendicular receiver lines, this design becomes a swath geometry (as shown in Figure 4a), one of the most common 3-D land acquisition geometries (Yilmaz, 2008; Liner, 2016). To mathematically represent the 3-D seismic data, a data cube $\mathcal{F} \in \mathbb{R}^{I_1 \times I_2 \times I_3 \times 1 \times 1}$ is acquired by a cross-spread, where each dimension represents I_1 time samples, I_2 receivers, and I_3 number of sources. However, the swath design has multiple source and receiver lines. As a result, the dimensions are now represented as $\mathcal{F} \in \mathbb{R}^{I_1 \times I_2 \times I_3 \times I_4 \times I_5}$, where I_4 and I_5 denote the number of receiver and source lines, respectively. To simplify the computational complexity of working with

Figure 4. 3-D land seismic acquisition.

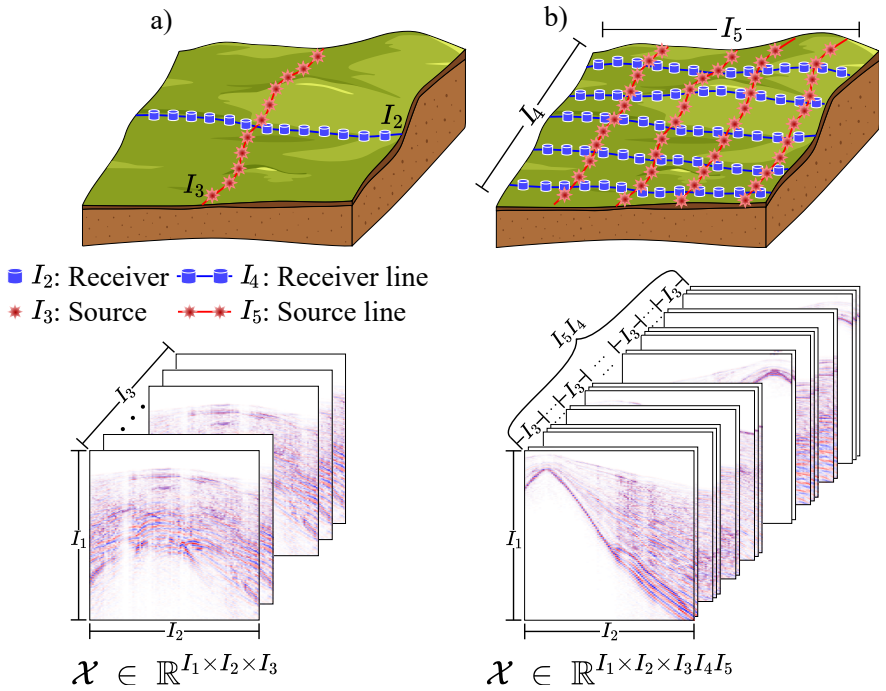

Note: (a) Cross-spread geometry with a single receiver and source line, generating the data cube $\mathcal{X} \in \mathbb{R}^{I_1 \times I_2 \times I_3}$. (b) Swath geometry composed of several receiver and source lines. The resulting data cube $\mathcal{X} \in \mathbb{R}^{I_1 \times I_2 \times I_3 I_4 I_5}$ is expressed as a concatenation of multiple cross-spread.

high-dimensional data, the data cube $\mathcal{F}$ is rearranged into $\mathcal{X} \in \mathbb{R}^{I_1 \times I_2 \times I_3 I_4 I_5}$, where all shot gathers are stacked along the third dimension (as shown in Figure 4b). The tensor notation used in this section is detailed in Table 3, based on tensor operations described in Kolda and Bader (2009) and its application on seismic data discussed in Popa et al. (2021).

The design of the sensing pattern depends on whether the problem involves removing receivers (trace reconstruction) or sources (shot gather reconstruction). A sampling vector $\boldsymbol{\phi} \in \{0, 1\}^M$ with dimensions equal to the number of receivers or sources defines the sensing pattern. The entries of $\boldsymbol{\phi}$, denoted as ϕ_i, determine whether the information is acquired. If $\phi_i = 0$, the receiver or source is removed from the data, while $\phi_i = 1$ indicates that it is

Table 3
Mathematical notation summary and definition of main operations used in this work.

Notation	**Description**
$\mathcal{X},\ \mathbf{X},\ \mathbf{x},\ x$	Tensor, matrix, vector, scalar
$\mathbf{1} \in \{1\}^{I_1}$	Vector with all elements in 1
$\mathcal{X} \in \mathbb{R}^{I_1 \times I_2 \times I_3}$	3-order tensor, with size $I_1 \times I_2 \times I_3$
$\text{diag}(\mathbf{x}) = \mathbf{x}\mathbf{1}^\top \odot \mathbf{I}$	Diagonal matrix obtained from $\mathbf{x}$, $\odot$ is the Hadamard product
$\mathbf{Y} = \mathbf{\Phi} \otimes \mathbf{X}$	Kronecker product between $\mathbf{\Phi} \in \mathbb{R}^{I_1 \times I_2}$ and $\mathbf{X} \in \mathbb{R}^{I_3 \times I_4}$, resulting in $\mathbf{Y} \in \mathbb{R}^{I_1 I_3 \times I_2 I_4}$
$\mathbf{X}_n \in \mathbb{R}^{I_n \times \tilde{I}_n}$	Mode-n unfolding matrix of $\mathcal{X}$. $\tilde{I}_n$ is the product of all dimensions except I_n
$\mathcal{Y} = \mathcal{X} \times_n \mathbf{\Phi}$	Mode-n product of $\mathcal{X} \in \mathbb{R}^{I_1 \times \cdots \times I_n \times \cdots \times I_N}$ and $\mathbf{\Phi} \in \mathbb{R}^{J \times I_n}$, resulting in $\mathcal{Y} \in \mathbb{R}^{I_1 \times \cdots \times J \times \cdots \times I_N}$, where $\mathbf{Y}_n = \mathbf{\Phi}\mathbf{X}_n$
$\|\|\mathcal{X}\|\|_2^2 = \sum x_{i,j,k}^2$	l_2-norm squared of the tensor $\mathcal{X}$, computed as the sum of the squared tensor elements

acquired. For practical purposes, a diagonal sampling matrix $\mathbf{\Phi} \in \{1, 0\}^{N \times N}$ is derived from $\boldsymbol{\phi}$ using the following two acquisition models:

5.2.1. Receiver removal. When removing receivers, the sampling vector $\boldsymbol{\phi} \in \{0, 1\}^{M=I_2}$ is used since I_2 is the total number of receivers. Once $\boldsymbol{\phi}$ is built, the sampling matrix $\mathbf{\Phi} \in \{1, 0\}^{I_2 \times I_2}$ representing the removed receivers can be obtained by:

$$\mathbf{\Phi} = \text{diag}(\boldsymbol{\phi}), \tag{3}$$

and the undersampled measurements are obtained via mode-n product defined in Lathauwer et al. (2000)

$$\mathcal{Y} = \mathcal{X} \times_2 \mathbf{\Phi}, \tag{4}$$

where Equation (4) represents the mode-2 product between the full data $\mathcal{X}$ and $\mathbf{\Phi}$. The undersampled measurements $\mathcal{Y} \in \mathbb{R}^{I_1 \times I_2 \times I_3 I_4 I_5}$ contains the removed receivers as columns in zero for each shot gather.

5.2.2. Source removal. When removing sources, the sampling vector $\boldsymbol{\phi} \in \{0,1\}^{M=I_3 I_5}$ is used, where $I_3 I_5$ is the total number of sources. However, the construction of $\mathbf{\Phi}$ differs because a single source generates as many shot gathers as the number of receiver lines. Therefore, to construct $\mathbf{\Phi}$ from $\boldsymbol{\phi}$, it is necessary to replicate each element ϕ_i as many times as the number of receiver lines using the Kronecker product

$$\mathbf{\Phi} = \mathrm{diag}(\boldsymbol{\phi} \otimes \mathbf{1}), \tag{5}$$

where $\mathbf{1} \in \{1\}^{I_4}$ since I_4 is the number of receiver lines. The resulting dimensions are $\mathbf{\Phi} \in \{1,0\}^{I_3 I_4 I_5 \times I_3 I_4 I_5}$, and $I_3 I_4 I_5$ represents the total number of shot gathers. Once $\mathbf{\Phi}$ is built, the undersampled measurements are obtained via mode-3 product

$$\mathcal{Y} = \mathcal{X} \times_3 \mathbf{\Phi}, \tag{6}$$

where the measurements $\mathcal{Y} \in \mathbb{R}^{I_1 \times I_2 \times I_3 I_4 I_5}$ contains the removed shot gathers as zero matrices.

The undersampling rate is conventionally used to determine the number of acquired receivers or sources by the sensing pattern. It is calculated as:

$$\delta_{\boldsymbol{\phi}} = \sum_{i=1}^{M} \frac{\phi_i}{M}. \tag{7}$$

For instance, when $\delta_{\boldsymbol{\phi}} = 0.7$, the 70 % of the total receivers/sources are acquired. After the measurements are acquired, an optimization problem is formulated to recover $\mathcal{X}^*$ from $\mathcal{Y}$

$$\mathcal{X}^* = \arg\min_{\mathcal{X}} ||\mathcal{Y} - \mathcal{X} \times_n \boldsymbol{\Phi}||_2^2 + \rho\mathcal{R}(\mathcal{X}), \tag{8}$$

where $n = 2$ and $n = 3$ stand for receiver and source removal, respectively.

In current formulations, the $\boldsymbol{\Phi}$ design often depends on geophysical parameters or data priors, such as the sparsity on a transformation domain or the low-rank structure. However, seismic data is highly dependent on the geological setting and can exhibit significant variations in its behavior, making the sparse and low-rank assumptions less accurate.

6. End-to-end methodology for designing seismic acquisition geometries

Typically, designing undersampled seismic acquisition geometries involves two stages: designing the sensing pattern and reconstructing the missing information. This work, however, proposes a different approach. Instead of optimizing these two stages separately, we developed an end-to-end (E2E) methodology that treats the entire process as one neural network. The first layer of the network identifies the optimal locations of sources and receivers for a given seismic survey, and the subsequent layers perform the computational algorithm to recover the missing data. By learning all the parameters through the reconstruction task over a training data set, the need to optimize the two stages sequentially is avoided.

This chapter explains the E2E methodology, which involves both sensing and reconstruction stages.

6.1. Sensing stage

The first step of the E2E methodology involves designing a trainable layer to model the missing receivers and sources, as described in Equations (4) and (6), respectively. To perform the sensing operation, the sensing pattern $\boldsymbol{\phi}$ must be optimized. This pattern is constrained to be binary and is obtained by applying a binary activation function B to a real-valued variable $\mathbf{w} \in \mathbb{R}^M$. Therefore, the final sensing pattern is given by

$$\boldsymbol{\phi} = B(\mathbf{w}), \tag{9}$$

where

$$B(w_i) = \begin{cases} 1, & \text{if } w_i \geq 0.5 \\ 0, & \text{if } w_i < 0.5, \end{cases} \tag{10}$$

and w_i denotes the i-th element of $\mathbf{w}$.

Additionally, this research proposes a low-dimensional representation of the latent weights $\mathbf{w}$, which is $\mathbf{w} = \mathbf{A}\mathbf{z}$, where $\mathbf{z} \in \mathbb{R}^d$ and $d \ll M$. The linear mapping $\mathbf{A}$ and the latent representation $\mathbf{z}$ are jointly learned through an E2E methodology that offers greater flexibility in training, albeit at the cost of an increased number of parameters. The acquisition process for the missing receivers or sources can thus be expressed as follows

$$\mathcal{Y} = \mathcal{M}_{\boldsymbol{\varphi}}(\mathcal{X}), \tag{11}$$

where $\boldsymbol{\varphi}$ represents the trainable parameters of the sensing layer corresponding to the low-dimensional vector $\mathbf{z}$ and the linear operation $\mathbf{A}$. The sensing stage in Figure 5 shows the acquisition process.

The derivative of B is zero throughout its domain and undefined at $w_i = 0.5$. Consequently, the gradient of Equation (10) becomes zero everywhere, which is not desirable for the standard back-propagation algorithm or chain rule (Yin et al., 2019). To overcome this issue, the Straight-Through Estimator (STE) strategy (Bengio, 2013; Hubara et al., 2016) was adopted, which involves substituting the zero derivatives of the activation function B in the chain rule with a surrogate function. Specifically, the clipped ReLU function $\mu(\mathbf{w})$ (Cai

Figure 5. Proposed E2E methodology for the design of compressive seismic acquisition geometries.

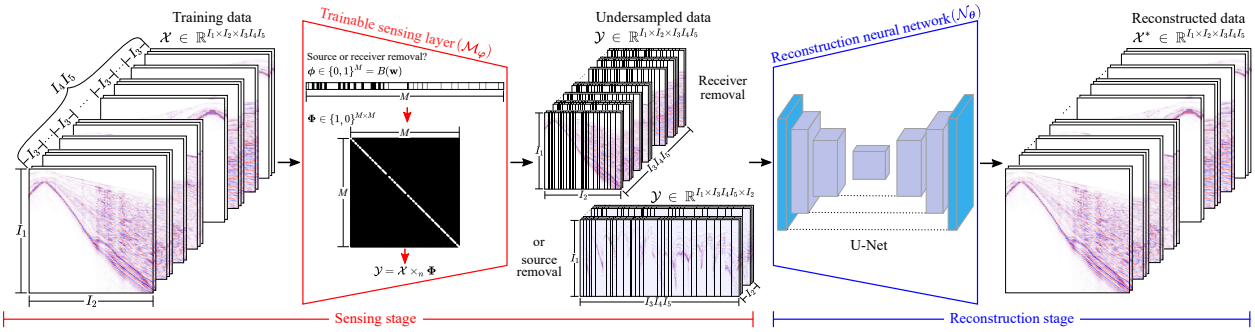

Note: The training data set $\mathcal{X}$ serves as the input to the model. Next, the trainable sensing layer $\mathcal{M}\varphi$ is designed to obtain undersampled data $\mathcal{Y} = \mathcal{M}\varphi(\mathcal{X})$, for missing receivers or sources. In the case of missing sources, the data is rearranged. Subsequently, the measurements $\mathcal{Y}$ are used as input to train the reconstruction neural network $\mathcal{N}_{\boldsymbol{\theta}}$, which generates an output tensor $\mathcal{X}^*$ that contains the recovered information.

et al., 2017) was employed as the STE

$$\mu(w_i) = \begin{cases} 1, & \text{if } w_i \geq 1 \\ w_i, & \text{if } 0 < w_i < 1 \\ 0, & \text{if } w_i \leq 0. \end{cases} \tag{12}$$

The concept behind Equation (12) involves utilizing the real-valued weights $\mathbf{w}$ to update the trainable parameters in the model rather than their binary counterpart $\boldsymbol{\phi}$. Moreover, the gradient clipping applied in Equation (12) strengthens the training of extremely deep neural networks (Cai et al., 2017; Pascanu et al., 2013). This feature is beneficial considering the architecture of the reconstruction network, as described in Section 6.2.

6.2. Reconstruction stage

The following stage in the E2E methodology involves reconstructing the missing information in $\mathcal{Y}$, as illustrated in the reconstruction stage in Figure 5. This stage utilizes a U-Net convolutional neural network (Ronneberger et al., 2015), denoted as $\mathcal{N}_{\boldsymbol{\theta}}$, with trainable weights $\boldsymbol{\theta}$ for the recovery task. The architecture of the U-Net varies based on whether the problem involves reconstructing traces (missing receivers) or shot gathers (missing sources):

6.2.1. Trace reconstruction. This work has opted for a 2-D U-Net architecture for trace reconstruction. This architecture comprises an encoding and decoding path connected through skip connections to enable the network to combine data features from various levels (Tang et al., 2022). Each encoder and decoder includes four pairs of 2-D convolutional layers. The difference is that the encoder utilizes max pooling operations for downsampling, whereas the decoder uses 2D transpose convolutions for upsampling. In addition, all convolutional layers use Rectified Linear Unit (ReLU) activation function, except the output layer, which employs a sigmoid function because seismic data range within the interval $[0, 1]$. The input to the 2-D U-Net is a data set with a size of $I_3 I_4 I_5 \times I_1 \times I_2 \times 1$, representing shots (batch) $\times$ time samples $\times$ receivers $\times$ channels, with undersampling carried out along the receiver's dimension. Figure 6 illustrates the neural network architecture.

6.2.2. Shot gather reconstruction. A 3D U-Net with an architecture similar to the 2D U-Net was employed to reconstruct shot gathers, but with the key difference that 3D convolutions are used instead. The input of the 3D U-Net is a data set with size

Figure 6. U-Net architecture for the reconstruction stage.

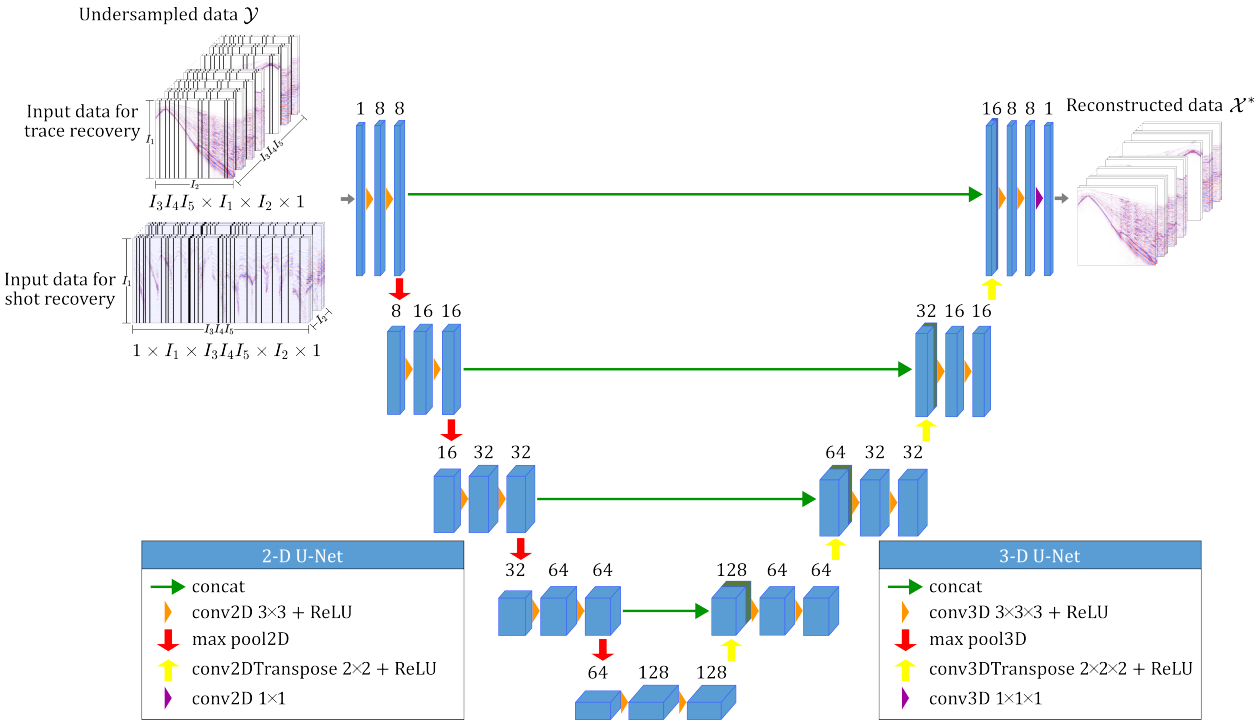

Note: The input data dimensions are shots (batch) × time samples × receivers × channels, and batch size × time samples × shots × receivers × channels for trace and shot recovery, respectively.

$1 \times I_1 \times I_3I_4I_5 \times I_2 \times 1$, representing batch size × time samples × shots × receivers × channels, respectively. The undersampling is carried out along the shot gather dimension. The swapping of the shots and receivers axis is due to the convolutional kernel being able to extract more spatial information from the data features than if the whole shot gather was kept as a zero matrix (see Figure 6).

After defining the sensing and reconstruction stages for either missing receivers or sources, they are trained simultaneously in an E2E methodology, which can be expressed mathematically as

$$\{\boldsymbol{\varphi}^*, \boldsymbol{\theta}^*\} = \arg\min_{\boldsymbol{\varphi},\boldsymbol{\theta}} \underbrace{||\mathcal{N}_{\boldsymbol{\theta}}(\mathcal{M}_{\boldsymbol{\varphi}}(\mathcal{X})) - \mathcal{X}||_2^2}_{\mathcal{L}_{\text{task}}} + \rho \underbrace{(\delta_0 - \delta_{\boldsymbol{\phi}})^2}_{\mathcal{R}(\boldsymbol{\phi})}, \tag{13}$$

where $\{\boldsymbol{\varphi}^*, \boldsymbol{\theta}^*\}$ represent the optimal weights of the sensing layer $\mathcal{M}_{\boldsymbol{\varphi}}$ and the reconstruction network $\mathcal{N}_{\boldsymbol{\theta}}$, respectively. The $\mathcal{L}_{\text{task}}$ represents the loss function of the reconstruction task, and $\mathcal{R}(\boldsymbol{\phi})$ is a regularizer to control the percentage of removed receivers or sources, which implicitly depends on $\boldsymbol{\varphi}$. The variable $\delta_{\boldsymbol{\phi}}$ was defined in Equation (7) as the undersampling rate depending on the trainable sensing pattern $\boldsymbol{\phi}$, and δ_0 denotes the desired undersampling rate. Thus, the sensing pattern $\boldsymbol{\phi}$ is updated until the constraint is satisfied, i.e., when $\delta_{\boldsymbol{\phi}} = \delta_0$.

Finally, the gradient of the loss function $\mathcal{L}$ of the whole model concerning $\boldsymbol{\varphi}$ is calculated using the chain rule

$$\frac{\partial \mathcal{L}}{\partial \boldsymbol{\varphi}} = \frac{\partial \mathcal{L}_{task}}{\partial \mathcal{N}_{\boldsymbol{\theta}}} \frac{\partial \mathcal{N}_{\boldsymbol{\theta}}}{\partial \mathcal{M}_{\boldsymbol{\varphi}}} \frac{\partial \mathcal{M}_{\boldsymbol{\varphi}}}{\partial \mu} \frac{\partial \mu}{\partial \mathbf{w}} \frac{\partial \mathbf{w}}{\partial \boldsymbol{\varphi}} + \rho \frac{\partial \mathcal{R}}{\partial \mu} \frac{\partial \mu}{\partial \mathbf{w}} \frac{\partial \mathbf{w}}{\partial \boldsymbol{\varphi}}. \tag{14}$$

Therefore, the design of the sensing pattern is directly influenced by the loss function of the reconstruction task and the one given by the physical constraints, such as the undersampling rate.

7. Seismic data sets

This section presents the synthetic and real data sets used for the simulations to evaluate the effectiveness of the proposed E2E methodology. It should be noted that the E2E methodology receives the acquired information (discrete data) as input and does not model the wave propagation in the optimization process.

7.1. Synthetic data sets modeled with Devito

Seismic numerical modeling involves simulating the propagation of waves in Earth's subsurface to predict the seismogram that would be recorded by a set of sensors based on the assumed subsurface structure (Carcione et al., 2002). This technique has various applications, including supporting field data interpretations, providing synthetic data, testing processing techniques and acquisition parameters, and advancing seismologists' understanding of wave propagation. Finite difference methods are commonly used for these applications (Zakaria and Penrose, 2000), along with other methods such as spectral and pseudo-spectral, limit element, finite element, and spectral element methods (Komatitsch and Martin, 2007). In this work, the finite difference methods with absorbing boundary conditions were implemented in the Python library `Devito` to perform seismic modeling in acoustic environments.

`Devito` was created to implement optimized computation for high-level problems such as finite difference, image processing, and machine learning. This package is based on `SymPy` and utilizes automated code generation and compilation to run optimized computational kernels on various computing platforms, including CPUs and GPUs.

7.1.1. Gas lens model. The simulated geological model comprises a low-velocity gas lens within a permeable sandstone reservoir. A thick layer of shale overlying it as a seal rock generates lateral truncation of the gas lens. These layers are folded to form an anticline structure. Above the shale, there is a poorly consolidated sediment layer. The 3D velocity model is presented in Figure 7.

Figure 7. Gas lens model.

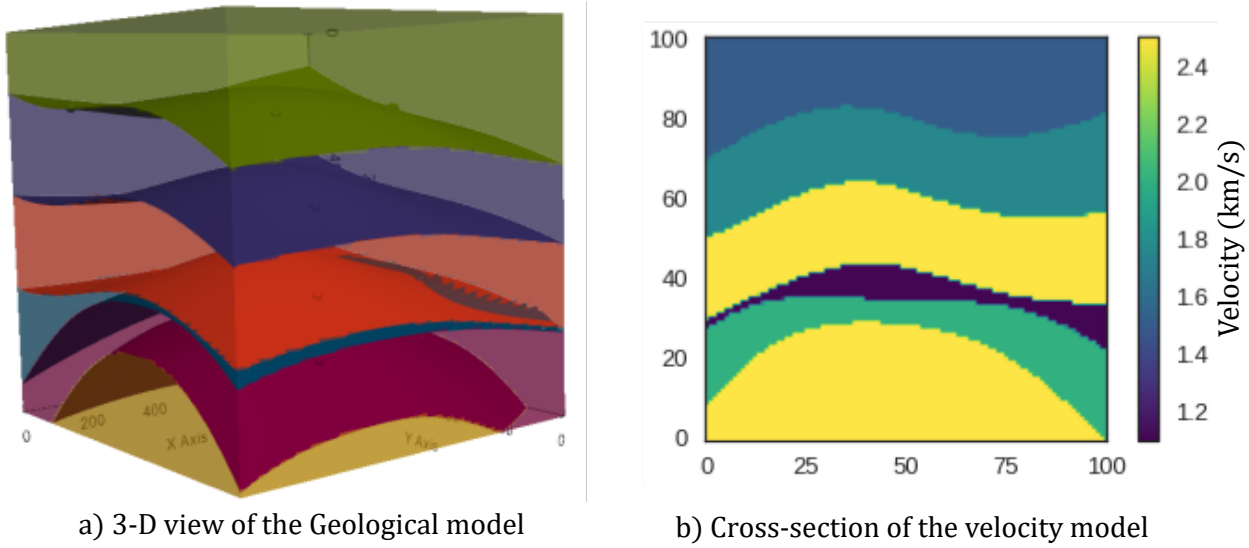

a) 3-D view of the Geological model

b) Cross-section of the velocity model

Note: a) 3D view of the model with the main anticline structure and b) truncation of the gas lens against the shale layers.

The simulated source is a Ricker wavelet with a peak frequency of 15 Hz ($f = 15$ Hz). The simulation began at 0 ms and ended at 1000 ms (1 second), with the source at a depth of 20 m.

The seismic acquisition geometry is a regular swath geometry that covers a rectangular patch of 1.5×1.5 km. The acquisition parameters are presented in Table 4, and a schematic

representation of the seismic survey is shown in Figure 10a.

7.1.2. Marmousi model. This model is based on a profile through the North Quenguela Trough in the Cuanza Basin in Angola (Figure 8). A geometric model containing 160 layers was created by introducing horizontal and vertical velocity gradients. This resulted in a 2-D grid with dimensions 3000 m in depth by 9200 m in offset (Versteeg, 1994).

Figure 8. Marmousi model.

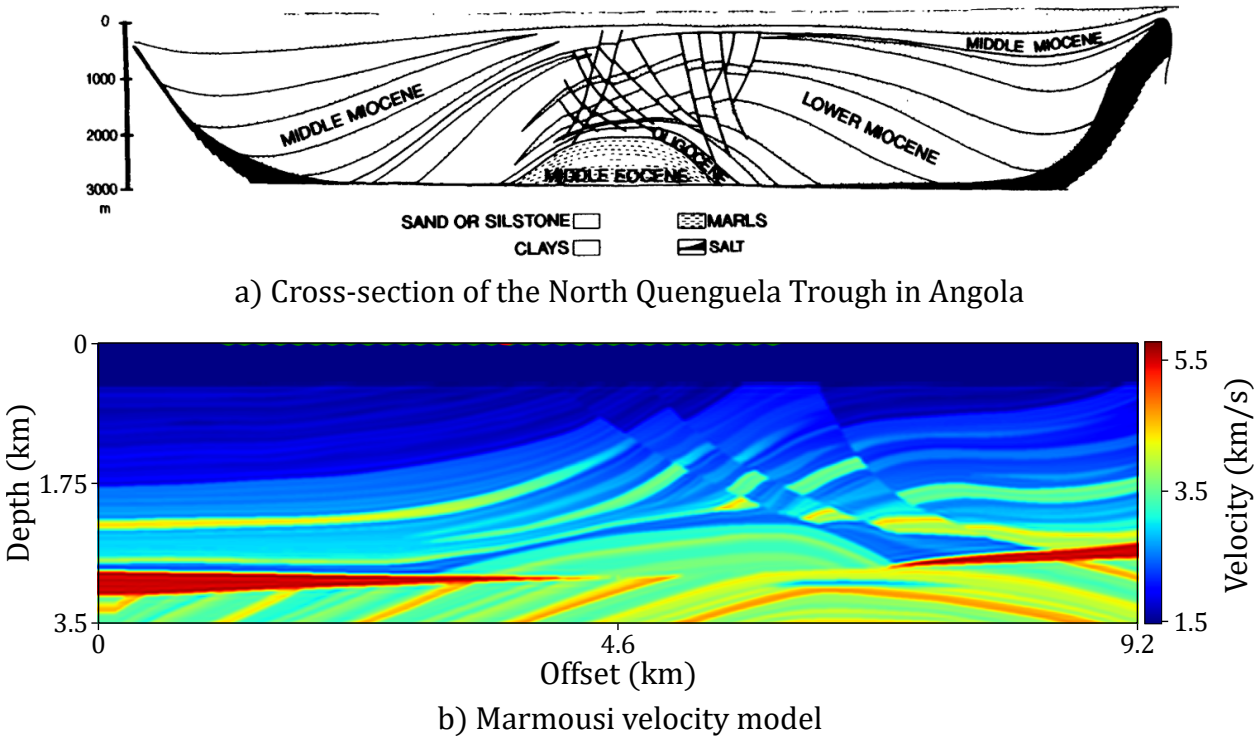

Note: a) Profile through the North Quenguela Trough in Angola, on which the structural model of Marmousi is based, and b) Marmousi velocity model, where the first layer represents the water table. Source: Versteeg (1994).

The simulated source is a Ricker wavelet with a peak frequency of 10 Hz ($f = 10$ Hz). The simulation began at 0 ms and ended at 3000 ms (3 seconds), with the source at a depth

of 20 m.

The seismic acquisition geometry is a 2-D regular end-on spread that covers a length of 5 km, with the source located 78 m away from the last receiver. The acquisition parameters are presented in Table 4, and a schematic representation of the seismic survey is shown in Figure 10b.

7.2. Synthetic data sets acquired from literature

7.2.1. SEAM Phase II. Synthetic-realistic data set built by the SEG Advanced Modeling Program (SEAM) during its second project, named "SEAM Phase II–Land Seismic Challenges" (Regone et al., 2017). The Foothills model is focused on mountainous regions with sharp topography at the surface and high geological complexity at depth (Figure 9), which makes this data set a challenge for seismic data reconstruction.

The seismic acquisition geometry is a regular swath geometry that covers a rectangular patch of 1.5×1.2 km, with a total sampled depth of 4100 ms. The acquisition parameters are presented in Table 4, and a schematic representation of the seismic survey is shown in Figure 10a.

7.3. Real data sets acquired from *Servicio Geológico Colombiano* (SGC)

7.3.1. 3-D Tenerife. Tenerife Field is located in the Middle Magdalena Valley Basin (MMVB) and is operated by Ecopetrol S.A. This field has a 3-D seismic survey of 22.61 km^2 with orthogonal geometry acquired by Compañía Geofísica Latinoamericana S.A (CGL). The objectives of Tenerife Field are to explore mixed traps in the Mugrosa and La Paz formations, as shown in Figure 11. The acquisition parameters for the full seismic

Figure 9. SEAM Phase II model.

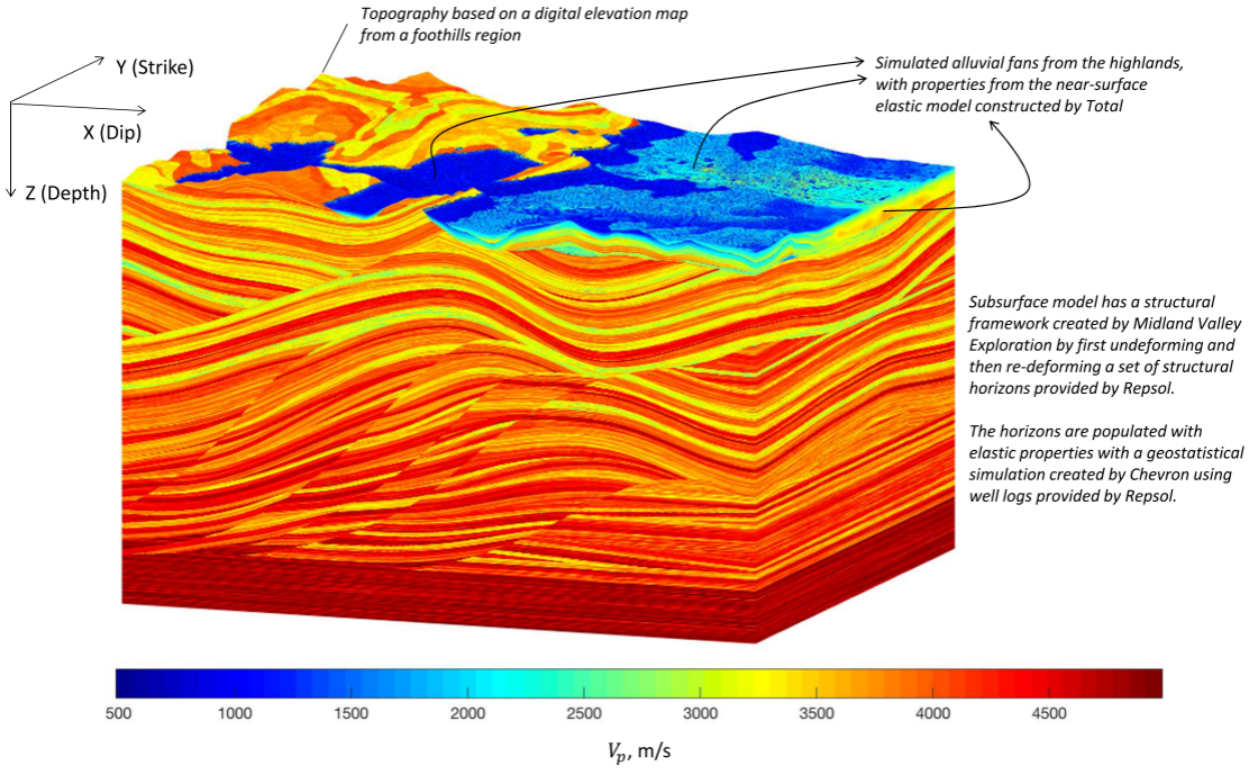

Note: Perspective view of the digital Foothills model. This 3D rendering of the grid of compressional wave velocity in the Foothills model shows the main structural features in strike and dip sections at the sides of the cube, along with the topography and the alluvial deposits near the surface. Source: (Regone et al., 2017).

Table 4
Seismic acquisition parameters for synthetic data sets.

Parameter	Gas lens model		Marmousi model		SEAM Phase II	
	Total	Interval	Total	Interval	Total	Interval
Time samples (I_1)	554	1.81 ms	2842	1.05 ms	1034	4 ms
Receivers (I_2)	128	20 m	128	39 m	128	10 m
Sources (I_3)	15	100 m	81	25 m	60	25 m
Receiver line (I_4)	15	100 m	1	25 m	12	100 m
Source line (I_5)	10	150 m	1	-	6	250 m
Total length in X (X)	1.5 km	-	7 km	-	1.5 km	-
Total length in Y (Y)	1.5 km	-	-	-	1.2 km	-
Total shots ($I_3I_4I_5$)	2250	-	81	-	4320	-

Figure 10. Plan view of the seismic acquisition geometry for synthetic data sets.

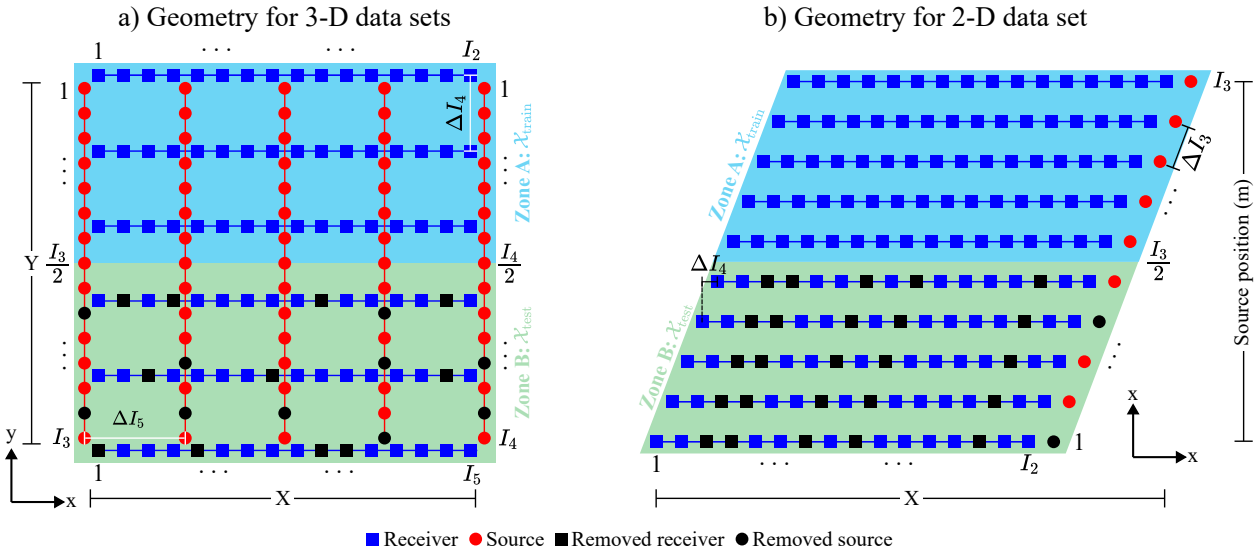

Note: Seismic acquisition geometry for a) Gas lens model and SEAM Phase II, and b) Marmousi model. The neural network is trained with data acquired in Zone A, and the designed acquisition pattern is tested in the new Zone B. The dimensions for each data set are referred to in Table 4.

Table 5
Seismic acquisition parameters for real data set.

Parameter	**3-D Tenerife**	
	Total	Interval
Time samples (I_1)	2501	-
Receivers (I_2)	252	20 m
Sources (I_3)	288	20 m
Receiver line (I_4)	19	280 m
Source line (I_5)	17	360 m
Total length of I_4 (X)	5.04 km	-
Total length of I_5 (Y)	5.76 km	-
Total shots ($I_3 I_4 I_5$)	93024	-

survey are presented in Table 5. However, the data provided consists of a pair source-receiver line with dimensions $2501 \times 252 \times 117$. The schematic representation of the seismic survey is shown in Figure 12.

Figure 11. Geology and structural setting from Tenerife Field.

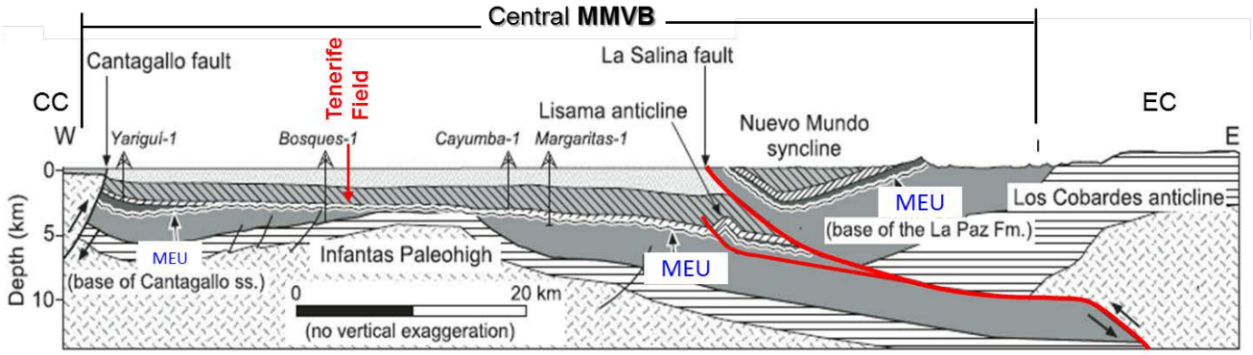

a) Regional structural section acoss the MMVB

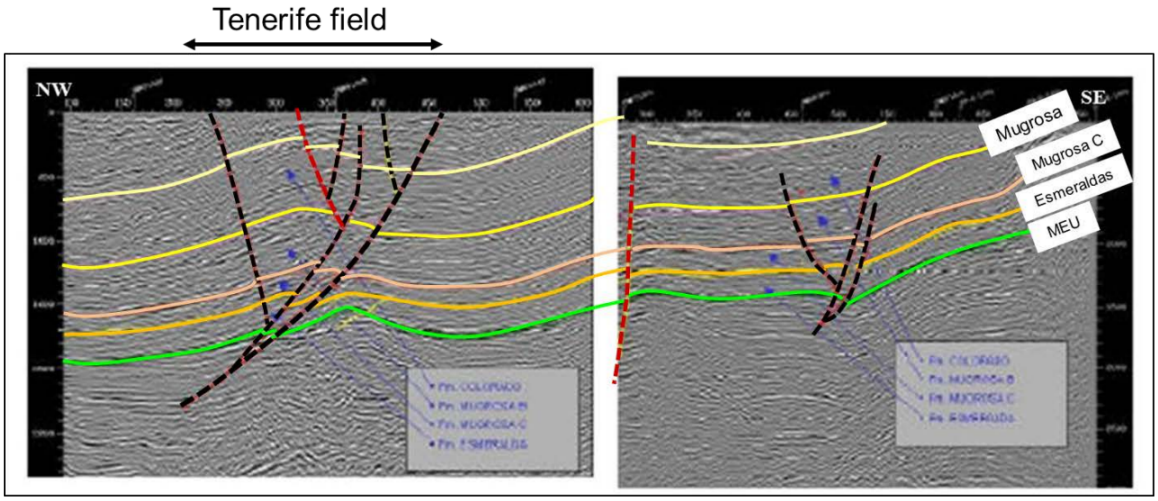

b) Seismic line with the structural interpretation of Tenerife Field

Note: a) The structurally-projected Tenerife Field is in red as a reference. Source: Gómez et al. (2005). b) The Tenerife structure is an asymmetric anticline faulted by a set of south-east-verging thrust faults and associated back thrusts. The normal-like faults are highlighted in red. Source: Velasquez-Espejo (2012).

Figure 12. Plan view of the seismic acquisition geometry for a real data set.

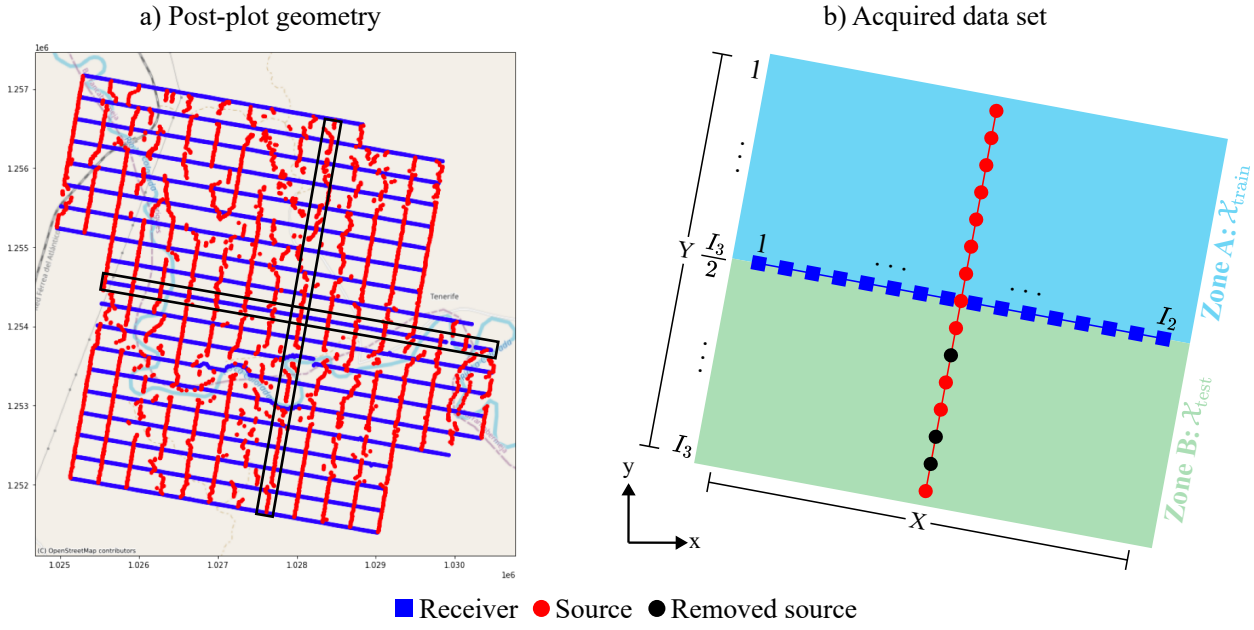

Note: a) Post-plot geometry for 3-D Tenerife seismic survey. The black box encloses the acquired cross spread. b) Schematic representation of the acquired cross-spread used for the simulations. The neural network is trained with data acquired in Zone A, and the designed acquisition pattern is tested in the new Zone B. The dimensions for each data set are referred to in Table 5.

8. Experimental setup

This section describes the experimental setup used to validate the proposed methodology through simulations. In addition, the computational specifications, evaluation metrics, and geometry design methods, as well as the data reconstruction algorithms of state-of-the-art, are also presented.

8.1. Computational specifications

The deep learning models are constructed using the Keras and Tensorflow libraries in Python version 3.9.15. All computations are carried out on an NVIDIA GeForce RTX 3080 Ti graphics processing unit with a memory capacity of 12 GB. The models are trained using a batch size of 16 and up to 500 epochs, balancing the training efficiency and convergence rate. To minimize the loss function, the Mean Squared Error (MSE), the Adam optimizer, is chosen as the optimization algorithm, as cited by (Allen, 1971). The learning rate is initially set to 0.001 and decreases by a factor of 0.9 when the validation loss function does not improve for 50 epochs.

8.2. Evaluation metrics

The reconstruction quality was evaluated by calculating the following metrics only on the removed information (traces or shots):

8.2.1. Mean Square Error (MSE). Mean Square Error (MSE) is the average difference between the pixels in the entire image. A high MSE value indicates a greater difference between the original and processed images. However, it is important to be cautious

when considering edges (Nadipally, 2019). The following equation shows how to calculate the MSE

$$\text{MSE} = \frac{1}{I_1 I_2} \sum_{i=1}^{I_1} \sum_{j=1}^{I_2} (x^*_{(i,j)} - x_{(i,j)})^2, \tag{15}$$

where $I_1 I_2$ represents the number of pixels, and $\mathbf{X}^*$ and $\mathbf{X}$ denote the reconstructed and ground truth shots, respectively.

8.2.2. Signal-to-Noise Ratio (SNR). The Signal-to-Noise Ratio (SNR) is the ratio between the power of the transmitted signal and the potential of the noise that corrupts it (Nadipally, 2019). This margin is expressed in decibels and can be calculated using the following equation

$$\text{SNR} = 10 \log \left(\frac{\sum_{i=1}^{I_1} \sum_{j=1}^{I_2} (x^*_{(i,j)})^2}{\text{MSE}} \right). \tag{16}$$

8.2.3. Peak-Signal-to-Noise Ratio (PSNR). The Peak Signal to Noise Ratio (PSNR) is a metric that compares a signal's maximum possible energy to the noise level. It is frequently used to assess the quality of the resulting image compared to the original image. A higher PSNR value indicates a better-reconstructed image quality Nadipally (2019). Mathematically, it can be defined as

$$\text{PSNR} = 10 \log \left(\frac{\text{máx} (\mathbf{X})^2}{\text{MSE}} \right), \tag{17}$$

where MAX_I refers to the maximum pixel value that can be represented in the image

8.2.4. Structural Similarity Index Measure (SSIM). The Structural Similarity Index (SSIM) is used to measure the similarity between two images, one of which is the reference image. In other words, it is defined mathematically to compare and measure the visual quality of an image concerning the original.

$$\text{SSIM} = \frac{(2\mu_x\mu_y + c_1)(2\sigma x_y + c_2)}{(\mu_x^2 + \mu_y^y + c_1)(\sigma_x^2 + \sigma_y^2 + c_2)}, \tag{18}$$

where $\mu_x = \frac{||\mathbf{X}||_2^2}{I_1 I_2}$, $\mu_y = \frac{||\mathbf{X}^*||_2^2}{I_1 I_2}$, σ_x is the standard deviation of $\mathbf{X}$ and σ_y is the standard deviation of $\mathbf{X}^*$, σ_{xy}^2 is the covariance of $\mathbf{X}$ and $\mathbf{X}^*$, c_1 and c_2 represent stabilization constants.

8.3. Methods for the design of compressive seismic acquisition geometries

The seismic acquisition geometry obtained with the proposed method was compared with literature sensing schemes commonly used to test reconstruction algorithms, including random, *jittered*, and uniform patterns (see Chapter 3). The parameters for the *jittered* undersampling were strategically selected to avoid Fourier-domain artifacts, as described by Hennenfent and Herrmann (2008) (i.e., $\xi = \gamma$). The sensing schemes were decimated using different undersampling rates ($\delta_{\boldsymbol{\phi}} = [0.9, 0.8, 0.7, 0.6, 0.5]$), with 0.5 being the most extreme case of undersampling evaluated.

8.4. Algorithms for seismic data reconstruction

Although this work is focused on the design of the compressive seismic geometry, different reconstruction algorithms were compared to analyze if the designed geometry can be imple-

mented using various methodologies for seismic data reconstruction. Based on the review of state-of-the-art algorithms presented in Chapter 4, three algorithms were implemented for seismic data recovery:

8.4.1. Sparsity-based. Sparsity is based on the fact that a signal, when transformed under a specific domain, concentrates its information in a few coefficients. The optimization problem involves solving the $\ell_2 - \ell_1$ problem, where the first term ensures data fidelity, and the second term induces sparsity. Thus, the Gradient Projection for Sparse Reconstruction (GPSR) algorithm was used to solve the sparse signal recovery problem from incomplete or noisy measurements (Figueiredo et al., 2007). To induce sparsity in the data, the 3-D Wavelet transform was implemented, which is used for analyzing and processing signals with both temporal and frequency components. It allows to breakdown of a signal into different frequency components, revealing information about the signal at different scales (Stéphane, 2009).

8.4.2. Consensus Equilibrium. This algorithm was developed by Goyes-Penafiel et al. (2021). It proposes incorporating various regularization operators to reconstruct missing shots using the principles of sparsity through an optimization problem $\ell_2 - \ell_1$ and denoising implementing the BM3D algorithm.

8.4.3. Fast marching. The Fast Marching Method is a numerical algorithm for solving partial differential equations (PDEs) in computational mathematics. In addition, it is often used to solve problems in physics, engineering, and computer graphics (Daru, 2000). The Fast Marching Method is an iterative algorithm that starts with an initial set

of points and then "marches"through the medium, calculating the distance to neighboring points at each iteration. The algorithm maintains a priority queue of points, with the points with the smallest distance from the initial set having the highest priority. Then, the algorithm iteratively extracts the point with the highest priority from the queue, updates the distances to its neighbors, and adds the neighbors to the queue if they have not been processed before (Daru, 2000; Kimmel and Sethian, 1996).

9. Simulations and results

This section compares the proposed methodology for designing compressive seismic acquisition geometries with traditional sensing schemes. The sensing schemes were also tested with state-of-the-art reconstruction algorithms to analyze the methodology's implementation with other algorithms. Additionally, an analysis is presented using different undersampling rates.

9.1. Results on methods for designing compressive seismic acquisition geometries

This section compares the sensing pattern designed with the E2E methodology with traditional sensing schemes (random, jittered, and uniform). To this end, the sensing layer $\mathcal{M}_{\boldsymbol{\phi}}$ was fixed for each sensing pattern, and only the reconstruction network $\mathcal{N}_{\boldsymbol{\theta}}$ was trained. The comparison aims to evaluate the performance of the E2E methodology compared to traditional sensing schemes in terms of accuracy and efficiency.

9.1.1. Missing receivers: Trace reconstruction. A seismic trace represents the signal measured by a single receiver over time. Removing receivers from the seismic acquisition is akin to recovering a column (seismic trace) in a shot-gather matrix. Two experiments were conducted while considering the source location to determine the optimal location of receivers to be removed for the different data sets. In the first experiment, the neural network was trained using the data acquired in Zone A (refer to Figure 10), while in the second, it was trained using data acquired only for a specific location of the source line. The objective was to study how the source location affects the receiver sensing pattern, as the information gathered by receivers depends on the direction of seismic waves. After the model was

Table 6
Quantitative results for Missing receivers - First experiment on SEAM Phase II data set.

δ_ϕ	**Traces***	**Random**			**Jittered**			**Uniform**			**This work**		
		PSNR	SNR	MSE	PSNR	SNR	MSE	PSNR	SNR	MSE	PSNR	SNR	MSE
0.9	13	32.22	7.26	0.62	33.31	8.26	0.47	34.12	9.15	0.39	**39.05**	**14.03**	**0.15**
0.8	26	31.41	6.44	0.74	32.28	7.32	0.59	33.68	8.76	0.43	**36.93**	**11.66**	**0.23**
0.7	38	30.69	5.85	0.86	31.51	6.70	0.71	33.10	8.32	0.49	**33.87**	**8.62**	**0.42**
0.6	51	29.74	4.83	1.07	30.59	5.73	0.87	31.55	6.27	0.71	**32.89**	**8.03**	**0.51**
0.5	64	28.84	4.29	1.31	29.91	4.92	1.02	30.18	5.37	0.97	**31.41**	**6.89**	**0.72**

Note: The results show the PSNR, SNR, and MSE metrics. Traces* is the number of removed traces. MSE values are scaled to 10^{-3}.

trained, the designed sensing pattern was replicated in Zone B (refer to Figure 10), and the reconstruction network $\mathcal{N}_{\boldsymbol{\theta}}$ was used to recover the missing seismic traces.

9.1.1.1. First experiment: Cross-spread. The E2E was trained and tested using data from a single receiver line and generated by only one source line (i.e., a cross-spread acquisition) in the SEAM Phase II data set. Specifically, the dimensions of the data set used for training and testing the model were $\mathcal{X}_{\text{train}} = \mathcal{X}_{\text{test}} = 128 \times 128 \times 30$, representing time samples $\times$ receivers $\times$ shots (refer to Figure 10a). In addition, the time dimension was resized due to the reconstruction neural network architecture. Table 6 presents the quantitative results for different undersampling rates, while Figure 13 shows the trace reconstruction for $\delta_{\boldsymbol{\phi}} = 0.5$. The designed pattern in this work is similar to a uniform scheme, but the first and last traces are not removed to preserve important information at the edges. Random and jittered schemes were also tested but performed lower than the designed and uniform patterns. This is because consecutive removal of traces in these schemes can create considerable gaps of missing information that make reconstruction difficult in some zones.

Figure 13. Trace reconstruction for the Missing receivers - First experiment on SEAM Phase II data set.

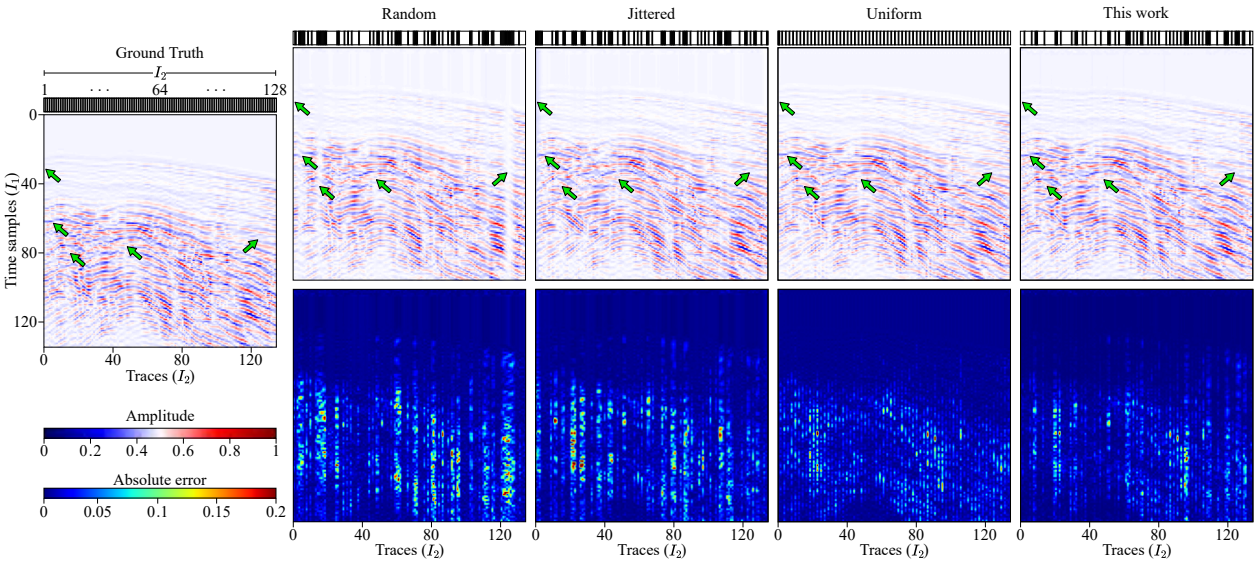

Note: To evaluate the performance of the E2E methodology, the comparison was made with different sensing schemes using an undersampling rate of $\delta_{\boldsymbol{\phi}} = 0.5$, which involved removing 64 of the 128 receivers. The sensing pattern $\boldsymbol{\phi} \in \{0,1\}^{128}$ for each shot gather is shown above it, with the removed and acquired receivers in black and white, respectively. Below each shot gather, the calculated metrics for the removed traces of the corresponding shot are displayed. The green arrow points to the main errors in the reconstruction.

9.1.1.2. Second experiment: Geometric analysis. The geometric analysis considers the source's location along the receiver line and the corresponding hyperbola of the resulting shot gather. Figure 14(a-c) displays the location of the source, and Figure 14(b-d) the acquired shot gather. Two notable points can be observed: First, the hyperbola's vertex follows the source's location along the receiver line. Therefore, if the source is at the end of the receiver line, the vertex of the hyperbola will be localized towards the right. The second point relates to the information acquired by the receivers, which differs if the sensors are next to the source or further away.

Considering the above, the simulations in this section involve learning the sensing pattern using training data with shot gathers in which the hyperbola is only located toward the left, center, or right. For the SEAM Phase II, the E2E was trained using a single cross-spread with dimensions of $\mathcal{X}\text{train} = \mathcal{X}\text{test} = 128 \times 128 \times 30$ for the training and testing data sets, as shown in Figure 10a. For the Marmousi model, the E2E was trained using a data set with dimensions of $\mathcal{X}\text{train} = \mathcal{X}\text{test} = 128 \times 128 \times 40$, as shown in Figure 10b. The time dimension was resized due to the reconstruction neural network architecture. Figure 15 shows the trace reconstruction of a shot gather of the SEAM Phase II data set, in which the hyperbola is located towards the left and its corresponding sensing pattern above. In the sensing pattern of this work, most of the removed traces are above or by the side of the vertex of the hyperbola, which is concordant as those receivers captured less information than the others. However, the random, jittered, and uniform traditional sensing schemes do

Figure 14. Geometric analysis of the shot gather according to the location of the source.

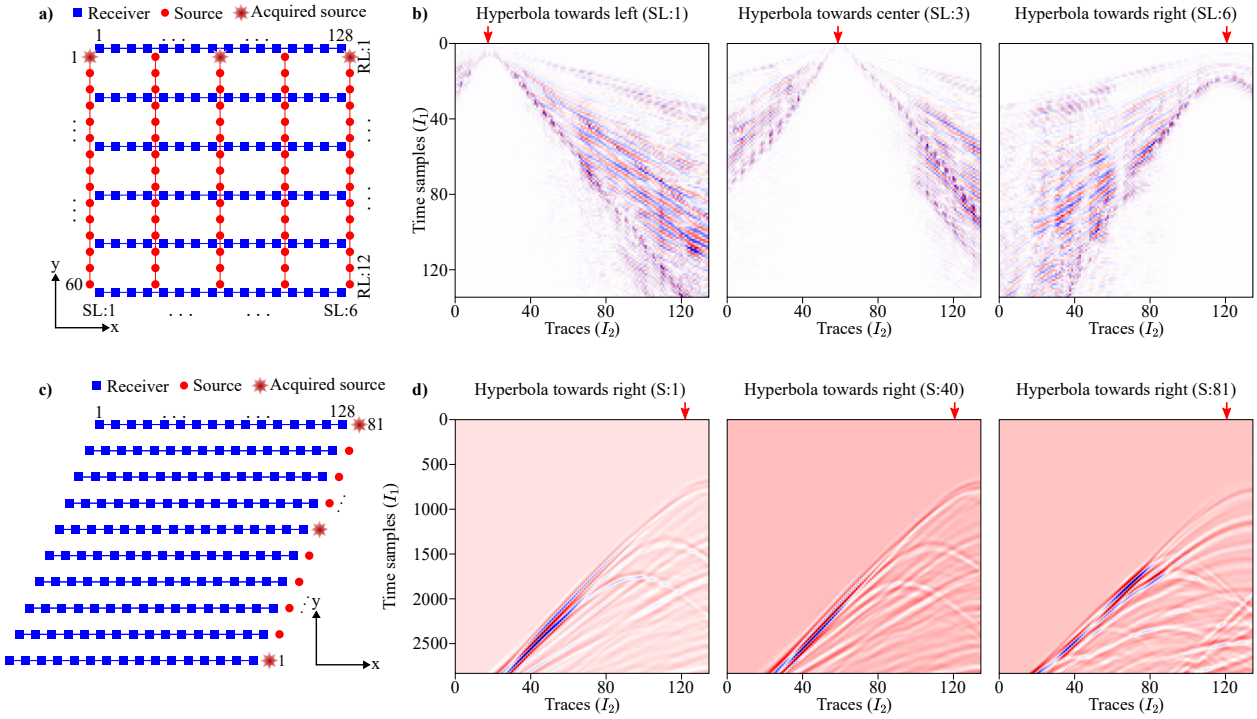

Note: Plan-view of the acquisition survey from a) SEAM Phase II and c) Marmousi data set, with the acquired sources highlighted. b) Shot gathers acquired by the highlighted sources from SL:1, SL:3, and SL:6 and recorded by RL:1, where SL and RL denote source and receiver lines, respectively. d) Shot gathers acquired by S:1, S:40, and S:81, where S denotes the source number. The red arrow points to the location of the source, which follows the vertex of the hyperbola.

Figure 15. Trace reconstruction for the Missing receivers - second experiment on SEAM Phase II data set.

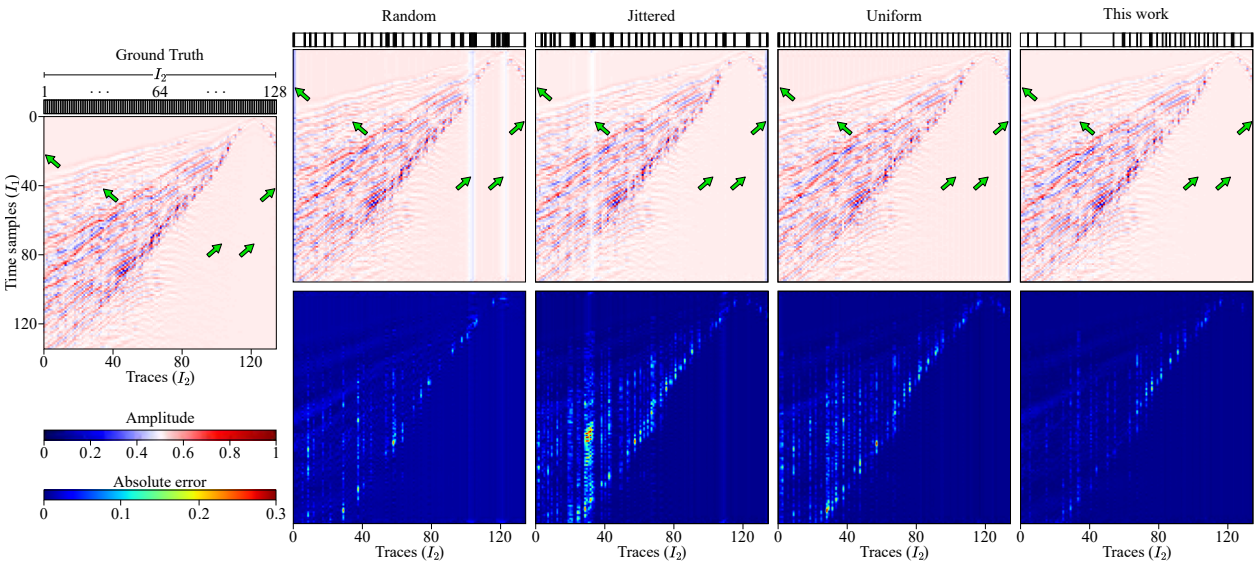

Note: The sensing pattern obtained with the E2E methodology was compared with different sensing schemes using an undersampling rate $\delta_{\boldsymbol{\phi}} = 0.7$, removing 38 of 128 receivers. Above each shot gather is shown the sensing pattern $\boldsymbol{\phi} \in \{0, 1\}^{128}$, with the removed and acquired receivers in black and white, respectively. The green arrow points to the main errors in the reconstruction.

not consider the spatial distribution of the data, which leads to low-quality reconstructions, as is reported in Table 7. Similar results were obtained for Marmousi model data set, as shown in Figure 16.

9.1.2. Missing sources: Shot gather reconstruction. A shot gather is a 2D representation that contains all the traces acquired by a single receiver line and generated by a single source. In 3D seismic acquisitions, there are several receiver lines, so a single source generates as many shot gathers as the number of receiver lines. Therefore, removing a source from a seismic survey represents a challenge in seismic data reconstruction, as it requires recovering several shot gathers.

Figure 16. Trace reconstruction for the Missing receivers - second experiment on Marmousi model data set.

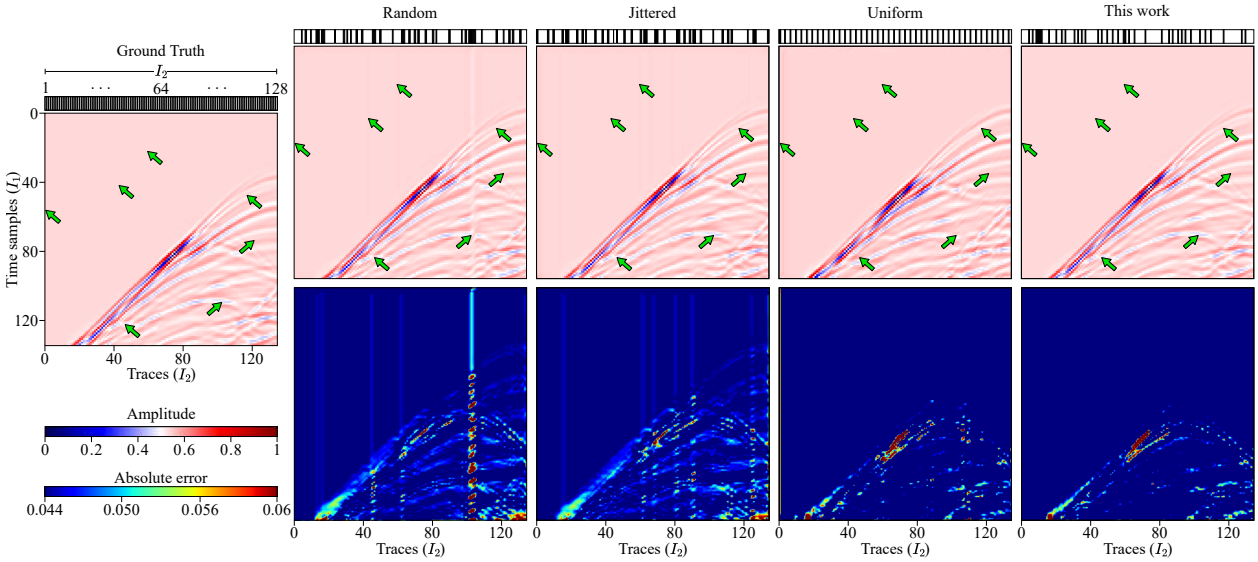

Note: The sensing pattern obtained with the E2E methodology was compared with different sensing schemes using an undersampling rate $\delta_{\phi} = 0.7$, removing 38 of 128 receivers. Above each shot gather is shown the sensing pattern $\phi \in \{0, 1\}^{128}$, with the removed and acquired receivers in black and white, respectively. The green arrow points to the main errors in the reconstruction.

Table 7
Quantitative results for Missing receivers - Second experiment on SEAM Phase II and Marmousi data sets.

	δ_{ϕ}	Traces*	Random			Jittered			Uniform			This work		
			PSNR	SNR	MSE	PSNR	SNR	MSE	PSNR	SNR	MSE	PSNR	SNR	MSE
SEAM Phase	0.9	13	31.67	4.68	0.64	31.82	5.02	0.66	33.38	6.82	0.39	**37.15**	**10.62**	**0.17**
	0.8	26	30.78	4.33	0.76	31.15	4.90	0.72	32.29	5.32	0.59	**36.40**	**9.48**	**0.22**
	0.7	38	30.49	3.75	0.88	30.55	4.18	0.85	31.39	4.70	0.76	**35.01**	**8.06**	**0.31**
	0.6	51	29.62	2.92	1.05	29.97	3.41	0.97	31.17	4.48	0.98	**33.76**	**6.70**	**0.41**
	0.5	64	29.22	2.47	1.16	29.62	2.89	1.07	31.11	4.39	0.75	**32.27**	**5.33**	**0.57**
Marmousi	0.9	13	31.25	7.15	0.55	33.71	7.98	0.42	34.08	8.95	0.41	**38.57**	**13.23**	**0.17**
	0.8	26	30.98	6.74	0.69	31.96	7.30	0.45	33.68	8.03	0.44	**37.25**	**11.58**	**0.29**
	0.7	38	29.85	6.25	0.76	31.03	6.66	0.61	32.91	7.92	0.53	**34.57**	**9.55**	**0.48**
	0.6	51	29.34	4.99	0.98	30.08	5.58	0.95	31.68	6.14	0.71	**33.27**	**8.78**	**0.64**
	0.5	64	28.02	3.57	1.25	29.01	4.54	1.37	30.34	5.00	0.99	**31.59**	**6.85**	**0.87**

Note: The results show the PSNR, SNR, and MSE metrics. Traces* is the number of removed traces. MSE values are scaled to 10^{-3}

To select the optimal location of sources to be removed, the E2E is trained using data acquired in Zone A (Figure 10a). The results after training include the optimal sensing pattern $\boldsymbol{\phi}$ and the reconstruction network $\mathcal{N}_{\boldsymbol{\theta}}$. The designed sensing pattern $\boldsymbol{\phi}$ indicates the best location for source removal, preserving the high quality of the reconstructed shot gathers. In Zone B (Figure 10a), the designed acquisition pattern $\boldsymbol{\phi}$ is replicated to acquire undersampled measurements $\mathcal{Y}$. The reconstruction network $\mathcal{N}_{\boldsymbol{\theta}}$ recovers the missing shot gathers. Similarly, comparisons with traditional random, jittered, and uniform sensing schemes were carried out using data in Zone A and B for training and testing, respectively. However, the main difference with the proposed design is that the sensing layer $\mathcal{M}\boldsymbol{\phi}$ was frozen for each sensing pattern, and only the reconstruction network $\mathcal{N}_{\boldsymbol{\theta}}$ was trained.

To analyze how the number of removed sources affects reconstruction quality, the E2E methodology was applied to both Gas lens and SEAM Phase II data sets with different undersampling rates $\delta_{\boldsymbol{\phi}} = [0.9, 0.8, 0.7, 0.6, 0.5]$. The best shot gather reconstructions for the Gas lens and SEAM Phase II data sets using an undersampling rate of $\delta_{\boldsymbol{\phi}} = 0.8$ are displayed in Figures 17 and 18, respectively. Reconstruction data from the E2E methodology and traditional sensing schemes were compared in time-space (T-X) and frequency-wavenumber (F-K) domains. Above each shot gather is shown the matrix form of the seismic survey, where the black and white circles represent the removed and the acquired sources, respectively. Table 8 presents the quantitative evaluation of the reconstruction quality using three metrics: PSNR, MSE, and Structural Similarity Index (SSIM) from Wang et al. (2004), which were computed only for the recovered shot gathers. These results are averaged over 50 reali-

Table 8
Quantitative results for shot gather reconstruction on Synthetic and SEAM Phase II data sets.

	δ_ϕ	Sources*	Shots*	Random			Jittered			Uniform			This work		
				PSNR	MSE	SSIM	PSNR	MSE	SSIM	PSNR	MSE	SSIM	PSNR	MSE	SSIM
Synthetic	0.9	7	49	27.59	1.75	0.889	28.29	1.55	0.899	29.02	0.71	0.908	**31.02**	**0.42**	**0.935**
	0.8	14	98	26.87	1.23	0.880	27.62	1.69	0.891	28.79	1.06	0.890	**30.73**	**0.71**	**0.925**
	0.7	21	147	26.09	2.29	0.867	27.12	1.92	0.887	27.63	1.72	0.881	**28.47**	**1.29**	**0.908**
	0.6	28	196	25.50	2.43	0.851	26.35	2.09	0.862	26.51	1.77	0.871	**26.95**	**1.69**	**0.889**
	0.5	35	245	23.71	2.98	0.836	23.84	2.16	0.843	24.58	1.94	0.856	**25.70**	**2.07**	**0.874**
SEAM	0.9	18	108	29.75	1.85	0.915	29.56	1.71	0.906	29.61	1.17	0.917	**31.05**	**0.56**	**0.954**
	0.8	36	216	26.48	2.54	0.867	26.87	2.21	0.849	27.43	2.11	0.856	**29.49**	**1.15**	**0.917**
	0.7	54	324	24.99	3.01	0.754	25.54	2.85	0.793	25.98	2.71	0.802	**27.15**	**2.01**	**0.889**
	0.6	72	432	23.76	3.92	0.692	24.19	3.97	0.781	24.35	3.82	0.788	**25.82**	**2.56**	**0.861**
	0.5	90	540	22.94	4.82	0.587	23.78	4.71	0.689	23.48	4.05	0.711	**24.05**	**3.15**	**0.855**

Note: The results show the PSNR, MSE, and SSIM metrics. Sources* and Shots* are the number of removed sources and shot gathers, respectively. MSE values are scaled to 10^{-3}.

zations for each undersampling rate. The lowest metrics were observed with random sensing, likely due to the consecutive removal of sources that made the reconstruction of shot gathers difficult. Although jittered sensing minimized the gaps in missing information, it still preserved some consecutive removed sources that reduced reconstruction quality. Conversely, the sensing pattern designed in this work and the uniform pattern produced the highest metric values. However, the designed pattern outperformed the uniform pattern by up to 2 dB due to the strategic selection of removed sources.

9.2. Results on reconstruction algorithms comparison

This section compares the reconstruction using state-of-the-art algorithms to analyze whether the designed geometry can be implemented using various methodologies for seismic data reconstruction. For this purpose, besides the reconstruction network $\mathcal{N}_{\boldsymbol{\theta}}$ proposed in this work, three iterative algorithms were implemented: one sparsity-based with GPSR, Consen-

Figure 17. Shot gather reconstruction for the Gas lens data set.

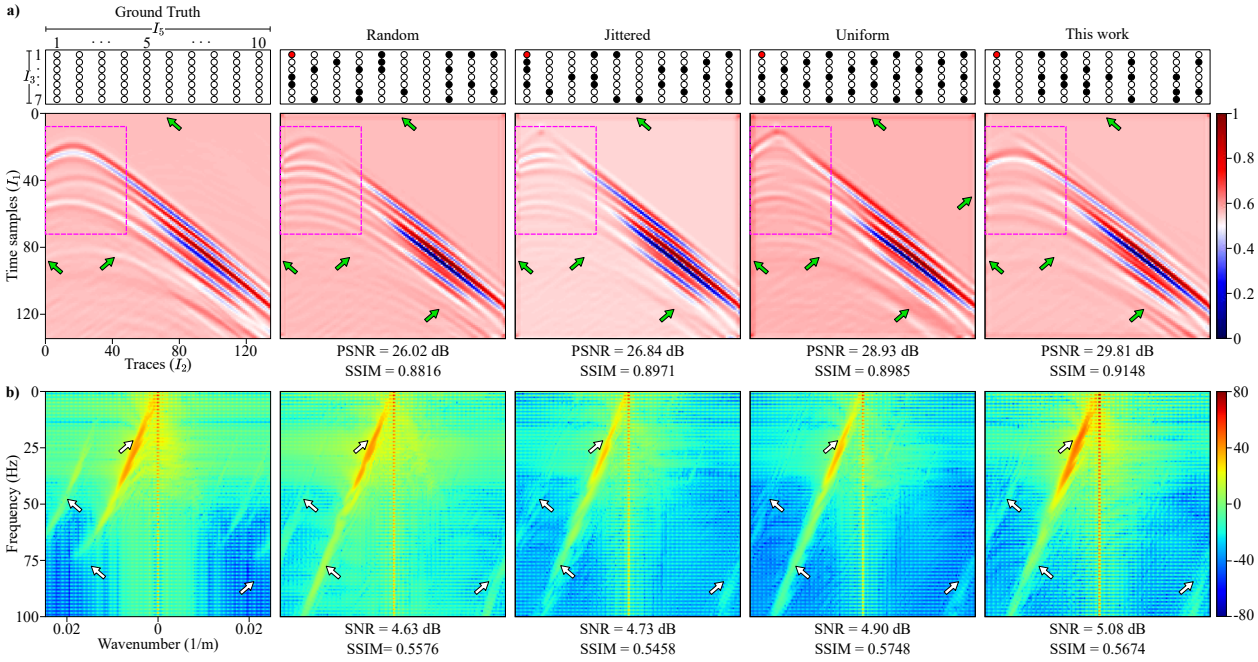

Note: The sensing pattern obtained with the E2E methodology was compared with different sensing schemes using an undersampling rate $\delta_{\boldsymbol{\phi}} = 0.8$. a) Time-space (T-X) domain of the original and reconstructed shot gather. Above each shot gather is shown a schematic plan view of the seismic survey, i.e., it represents the sensing pattern $\boldsymbol{\phi} \in \{0,1\}^{I_3 I_5}$ rearranged in form for source lines. The white and black circles represent the acquired and removed sources, respectively, and the red one is the source from which the reconstructed shot gather. b) Frequency-wavenumber (F-K) domain of the original and reconstructed shot gather. Below each shot gather is shown the reconstruction metrics. The green and white arrows point to the main errors in the reconstruction.

Figure 18. Shot gather reconstruction for the SEAM Phase II data set.

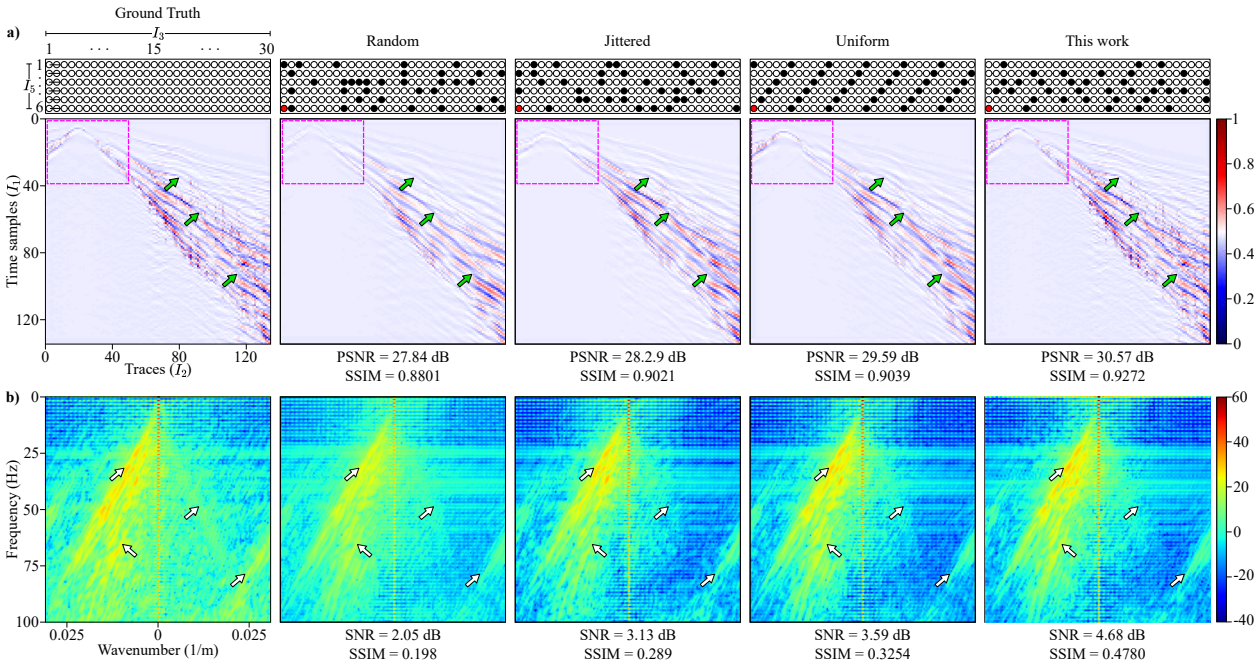

Note: The sensing pattern obtained with the E2E methodology was compared with different sensing schemes using an undersampling rate $\delta_{\boldsymbol{\phi}} = 0.8$. a) Time-space (T-X) domain of the original and reconstructed shot gather. Above each shot gather is shown a schematic plan view of the seismic survey, i.e., it represents the sensing pattern $\boldsymbol{\phi} \in \{0,1\}^{I_3 I_5}$ rearranged in form for source lines. The white and black circles represent the acquired and removed sources, respectively, and the red one is the source from which the reconstructed shot gather. b) Frequency-wavenumber (F-K) domain of the original and reconstructed shot gather. Below each shot gather is shown the reconstruction metrics. The green and white arrows point to the main errors in the reconstruction.

sus Equilibrium, and Fast Matching. The data set used for the simulations was a cross-spread from 3-D Tenerife (refer to Figure 12b) resized to $256 \times 256 \times 64$ to decrease the computational resources required to run the iterative algorithms. In addition, the undersampling rate was $\delta_{\boldsymbol{\phi}} = 0.6$, which means that 26 shots were removed. The sensing patterns tested were the one designed with the E2E methodology and the traditional sensing schemes such as random, jittered, and uniform.

Figures 19, 20, 22, and 21 show the shot gather reconstructions using the reconstruction network $\mathcal{N}_{\boldsymbol{\theta}}$ proposed in this work, as well as GPSR, Consensus Equilibrium, and Fast Marching algorithms, respectively. Additionally, Table 9 presents the quantitative results for each algorithm. It is worth highlighting that the recovery network $\mathcal{N}_{\boldsymbol{\theta}}$ outperforms the iterative algorithms regarding the reconstruction quality, demonstrating the advantages of Deep Learning for seismic data interpolation. Furthermore, the sensing pattern designed with the E2E methodology achieves higher metrics for all the reconstruction algorithms than traditional random, jittered, and uniform sensing schemes by up to 1 dB in PSNR. This confirms the possibility of incorporating these reconstruction strategies with the proposed methodology for seismic survey design.

Table 9
Quantitative results for shot gather reconstruction on 3-D Tenerife data sets.

Algorithm	**Random**			**Jittered**			**Uniform**			**This work**		
	PSNR	MSE	SSIM	PSNR	MSE	SSIM	PSNR	MSE	SSIM	PSNR	MSE	SSIM
Network ($\mathcal{N}_{\boldsymbol{\theta}}$)	28.59	1.72	0.896	29.55	1.42	0.923	29.69	1.31	0.931	**30.98**	**1.22**	**0.945**
GPSR	25.01	2.12	0.859	26.62	1.68	0.871	27.05	1.52	0.884	**28.73**	**1.35**	**0.921**
Fast Marching	23.55	2.98	0.814	24.46	2.57	0.832	25.51	2.12	0.849	**26.98**	**1.93**	**0.868**
Consensus	22.58	3.05	0.798	23.41	2.66	0.814	24.63	2.32	0.837	**24.47**	**2.09**	**0.845**

Note: The results show the PSNR, MSE, and SSIM metrics for a total of 26 shots ($\delta_{\boldsymbol{\phi}} = 0.6$). MSE values are scaled to 10^{-3}.

Figure 19. Shot gather reconstruction for the 3-D Tenerife data set using the reconstruction network $\mathcal{N}_{\boldsymbol{\theta}}$ of this work.

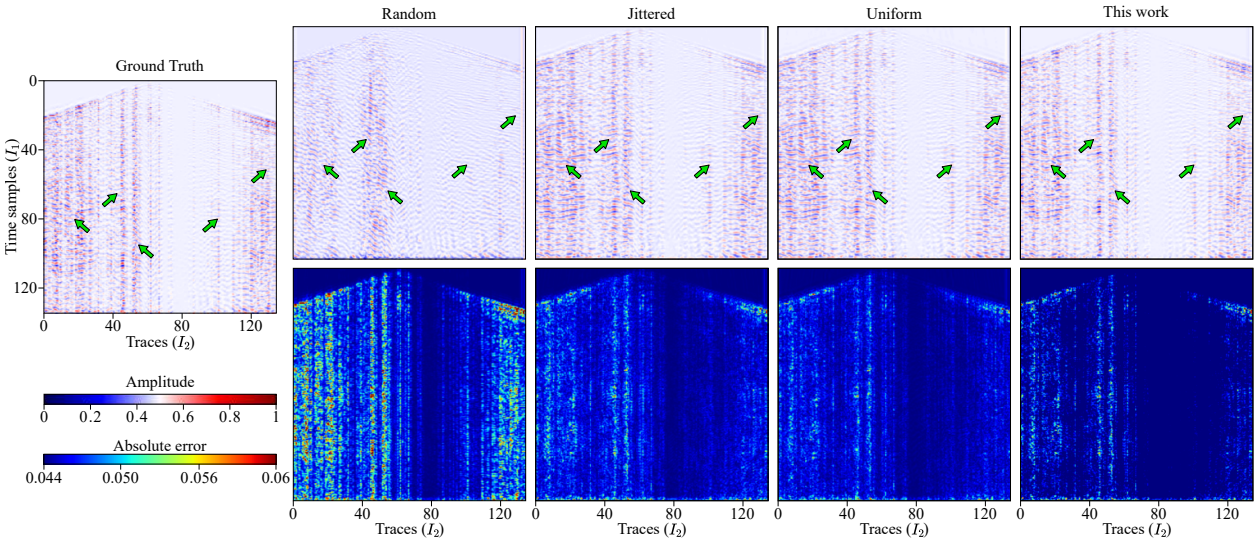

Note: The sensing pattern obtained with the E2E methodology was compared with different sensing schemes using an undersampling rate $\delta_{\boldsymbol{\phi}} = 0.6$, removing 26 of 64 sources. The green arrow points to the main errors in the reconstruction.

Figure 20. Shot gather reconstruction for the 3-D Tenerife data set using GPSR.

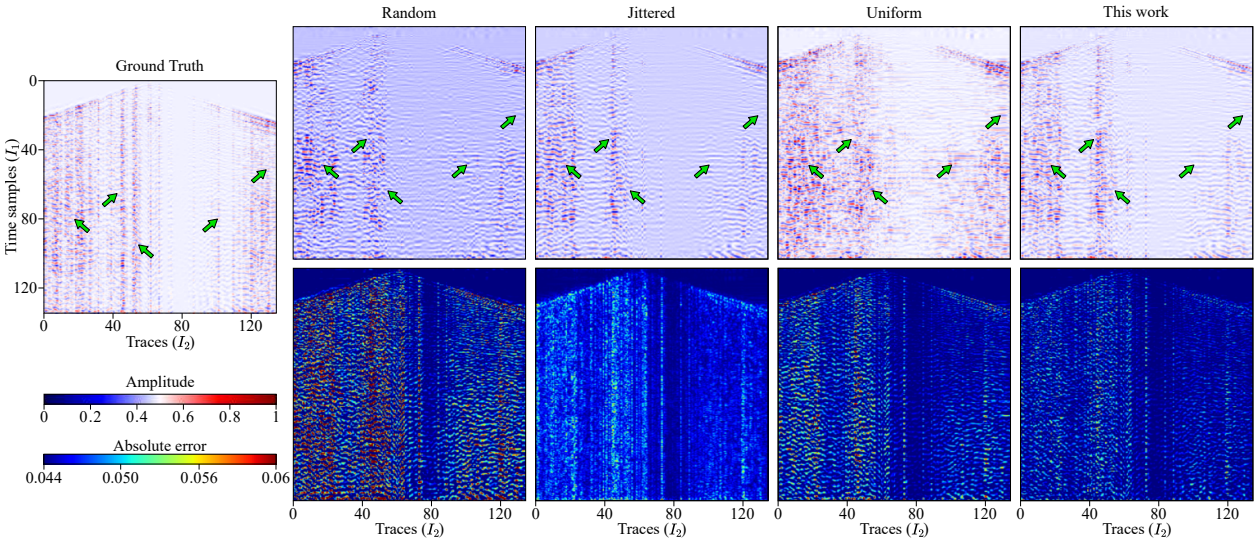

Note: The sensing pattern obtained with the E2E methodology was compared with different sensing schemes using an undersampling rate $\delta_\phi = 0.6$, removing 26 of 64 sources. The green arrow points to the main errors in the reconstruction.

Figure 21. Shot gather reconstruction for the 3-D Tenerife data set using Fast Marching.

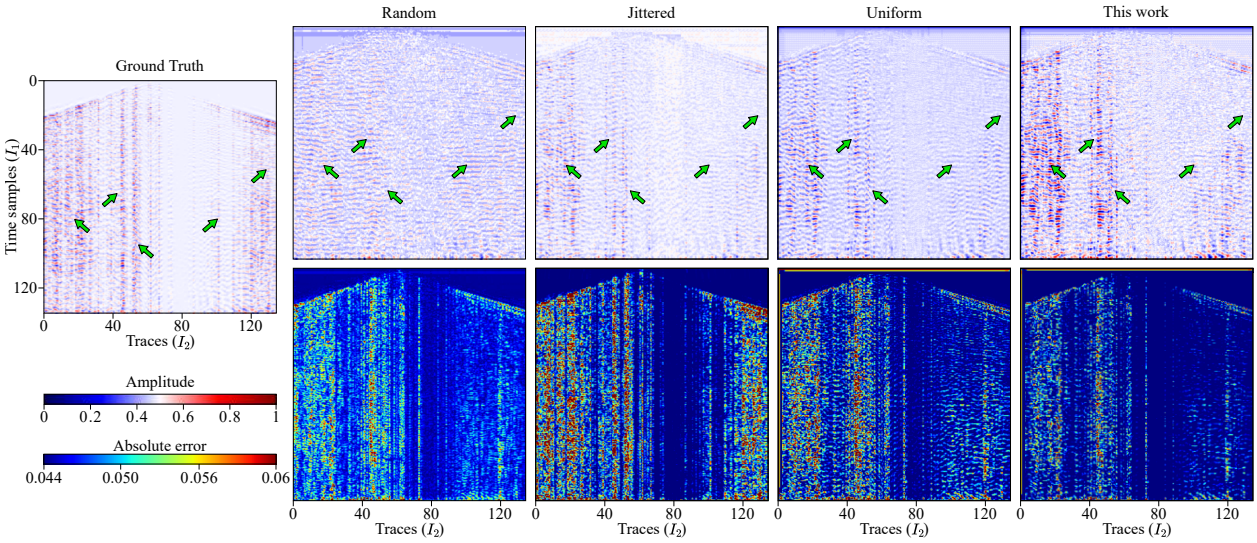

Note: The sensing pattern obtained with the E2E methodology was compared with different sensing schemes using an undersampling rate $\delta_\phi = 0.6$, removing 26 of 64 sources. The green arrow points to the main errors in the reconstruction.

Figure 22. Shot gather reconstruction for the 3-D Tenerife data set using Consensus Equilibrium.

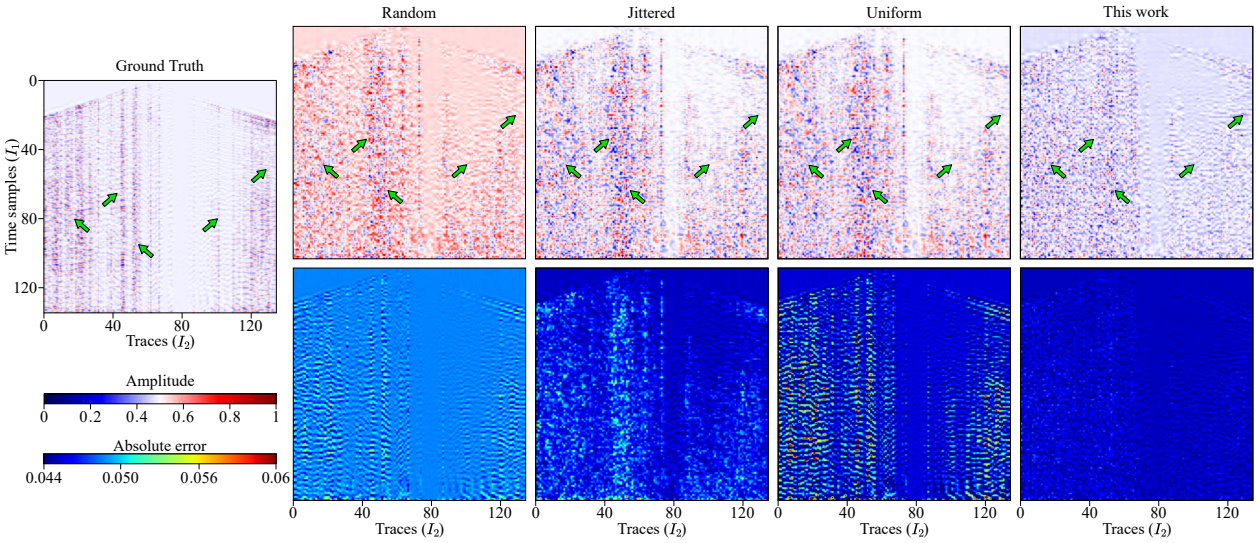

Note: The sensing pattern obtained with the E2E methodology was compared with different sensing schemes using an undersampling rate $\delta_\phi = 0.6$, removing 26 of 64 sources. The green arrow points to the main errors in the reconstruction.

10. Conclusions

This work proposes a methodology for designing undersampled seismic surveys using a deep learning model. The model includes a trainable sensing layer and a reconstruction network jointly trained in an end-to-end optimization framework.

The mathematical acquisition model was first formulated using vector and tensor notation for 2-D and 3-D seismic surveys. The vector notation helped to implement the sparsity-based algorithms, while the tensor model allowed for the representation of the different dimensions presented in seismic geometries, such as receivers, sources, receiver lines, and source lines. With this formulation, Objective 1 was achieved.

Considering the previously formulated acquisition model, an end-to-end methodology was developed to jointly learn an optimized seismic design and the seismic data reconstruction. Firstly, a trainable binary layer was designed to learn the optimal locations of receivers and sources to be removed for a specific seismic survey. This layer includes a regularization parameter to control the number of receivers/sources to eliminate. Next, a reconstruction deep neural network was implemented to recover the missing information removed by the sensing pattern. Using this E2E methodology, an optimal sensing pattern was obtained and could be implemented in a seismic acquisition where the geological setting is similar to the training data set. The development of the E2E methodology helped achieve Objective 2.

Three synthetic data sets were generated to train and test the E2E model. The first is a 3-D orthogonal seismic data set obtained from a geological model with velocity anomalies

due to the presence of gas lenses. The other two correspond to the state-of-the-art Marmousi and SEAM Phase II models, representing high structural and stratigraphic complexity in land and marine environments. The seismic data set for SEAM Phase II is a 3-D orthogonal geometry, while the Marmousi model is a 2-D end-on spread. Regarding the real data set, a single cross-spread was acquired from the *Servicio Geológico Colombiano* of the 3-D Tenerife seismic survey. The generation of these data sets allowed us to achieve Objective 3.

The sensing pattern obtained with the proposed E2E methodology was compared with traditional random, jittered, and uniform sensing schemes. The results showed that the selection of receivers and sources to remove directly affects the quality of the reconstructed seismic data. Thus, the sensing pattern obtained outperformed the traditional sensing schemes, improving the reconstruction quality by up to 4 and 2 dB in PSNR for trace and shot gather reconstruction, respectively. In addition, the proposed sensing pattern was compared with traditional sensing schemes using state-of-the-art reconstruction algorithms such as sparsity-based, Consensus Equilibrium, and Fast Marching. The results confirm that the proposed seismic survey design can be incorporated into these reconstruction algorithms and still outperforms the reconstruction quality with the traditional sensing schemes. This validation helped achieve Objective 4.

To summarize, optimizing seismic surveys can reduce overall acquisition costs and environmental impacts by up to 50 % in real-world applications.

11. Future works

For future works, we propose to include different regularizers in the optimization problem according to acquisition constraints, such as complex topography, water bodies, and social restrictions that prevent localizing receivers and sources in some specific places. Additionally, it is important to analyze the effect of the optimized seismic survey on the whole seismic processing workflow, including amplitude processing, velocity analysis, and stacking.

References

Allen, D. M. (1971). Mean square error of prediction as a criterion for selecting variables. *Technometrics*, 13(3):469–475.

Alzubaidi, L., Zhang, J., Humaidi, A. J., Al-Dujaili, A. Q., Duan, Y., Al-Shamma, O., Santamaría, J., Fadhel, M. A., Al-Amidie, M., and Farhan, L. (2021). Review of deep learning: concepts, cnn architectures, challenges, applications, future directions. *Journal of Big Data*, 8:53.

Bacca, J., Gelvez-Barrera, T., and Arguello, H. (2021). Deep coded aperture design: An end-to-end approach for computational imaging tasks. *IEEE Transactions on Computational Imaging*, 7:1148–1160.

Baraniuk, R. G. and Steeghs, P. (2017). Compressive sensing: A new approach to seismic data acquisition. *The Leading Edge*, 36(8):642–645.

Bengio, Y. (2013). Estimating or propagating gradients through stochastic neurons.

Bhuiyan, M. and Sacchi, M. (2015). Optimization for sparse acquisition. volume 34, pages 254–259. Society of Exploration Geophysicists.

Blacquiere, G. and Nakayama, S. (2019). Optimum seismic acquisition geometry design with the help of artificial intelligence. pages 117–121. Society of Exploration Geophysicists.

Cai, R., Zhao, Q., She, D.-P., Yang, L., Cao, H., and Yang, Q.-Y. (2014). Bernoulli-based random undersampling schemes for 2d seismic data regularization. *Applied Geophysics*, 11:321–330.

Cai, Z., He, X., Sun, J., and Vasconcelos, N. (2017). Deep learning with low precision by half-wave gaussian quantization. pages 5406–5414. IEEE.

Campman, X., Tang, Z., Jamali-Rad, H., Kuvshinov, B., Danilouchkine, M., Ji, Y., Walk, W., and Smit, D. (2017). Sparse seismic wavefield sampling. *The Leading Edge*, 36:654–660.

Carcione, J. M., Herman, G. C., and ten Kroode, A. P. E. (2002). Seismic modeling. *GEOPHYSICS*, 67(4):1304–1325.

Chai, X., Tang, G., Wang, S., Peng, R., Chen, W., and Li, J. (2020). Deep Learning for Regularly Missing Data Reconstruction. *IEEE Transactions on Geoscience and Remote Sensing*, 58(6):4406–4423.

Chaouch, A. and Mari, J. L. (2006). 3-D Land Seismic Surveys: Definition of Geophysical Parameter. *Oil and Gas Science and Technology - Revue de l'IFP*, 61(5):611–630.

Chen, Y., Huang, W., Zhang, D., and Chen, W. (2016). An open-source matlab code package for improved rank-reduction 3d seismic data denoising and reconstruction. *Computers & Geosciences*, 95:59–66.

Daru, V. (2000). Level set methods and fast marching methods – evolving interfaces in computational geometry, fluid mechanics, computer vision, and materials science by j.a.

sethian (cambridge university press, cambridge, uk, 1999, 2nd edition, 378 pp.). *European Journal of Mechanics - B/Fluids*, 19:531–532.

Djikpesse, H. A., Khodja, M. R., Prange, M. D., Duchenne, S., and Menkiti, H. (2012). Bayesian survey design to optimize resolution in waveform inversion. *GEOPHYSICS*, 77:R81–R93.

Evans, B. J. (1997). *A Handbook for Seismic Data Acquisition in Exploration*. Society of Exploration Geophysicists.

Figueiredo, M. A. T., Nowak, R. D., and Wright, S. J. (2007). Gradient projection for sparse reconstruction: Application to compressed sensing and other inverse problems. *IEEE Journal of Selected Topics in Signal Processing*, 1(4):586–597.

Galvis, L., Ramírez, J. M., Vargas, E., Villarreal, O., Agudelo, W., and Arguello, H. (2020). Reconstruction of 2D Seismic Wavefields from Nonuniformly Sampled Sources. *Electronic Imaging*, 2020(14):307–307.

Goyes-Penafiel, P., Vargas, E., Correa, C. V., Agudelo, W., Wohlberg, B., and Arguello, H. (2021). A Consensus Equilibrium Approach for 3-D Land Seismic Shots Recovery. *IEEE Geoscience and Remote Sensing Letters*, (June):1–5.

Guo, Y. and Sacchi, M. D. (2020). Data-driven time-lapse acquisition design via optimal receiver-source placement and reconstruction. volume 2020-October, pages 66–70. Society of Exploration Geophysicists.

Gómez, E., Jordan, T. E., Allmendinger, R. W., Hegarty, K., and Kelley, S. (2005). Syntectonic cenozoic sedimentation in the northern middle magdalena valley basin of colombia and implications for exhumation of the northern andes. *GSA Bulletin*, 117(5-6):547–569.

Hennenfent, G. and Herrmann, F. J. (2008). Simply denoise: Wavefield reconstruction via jittered undersampling. *GEOPHYSICS*, 73(3):V19–V28.

Hinojosa, C., Bacca, J., and Arguello, H. (2018). Coded aperture design for compressive spectral subspace clustering. *IEEE Journal of Selected Topics in Signal Processing*, 12(6):1589–1600.

Hubara, I., Courbariaux, M., Soudry, D., El-Yaniv, R., and Bengio, Y. (2016). Binarized neural networks. In Lee, D., Sugiyama, M., Luxburg, U., Guyon, I., and Garnett, R., editors, *Advances in Neural Information Processing Systems*, volume 29. Curran Associates, Inc.

Jacome, R., Hernandez-Rojas, A., and Arguello, H. (2022). Probabilistic regularization for end-to-end optimization in compressive imaging. In *Imaging and Applied Optics Congress 2022 (3D, AOA, COSI, ISA, pcAOP)*, page CW1B.1. Optica Publishing Group.

Jamali-Rad, H., Kuvshinov, B., Tang, Z., and Campman, X. (2016). Deterministically subsampled acquisition geometries for optimal reconstruction. pages 1–5. European Association of Geoscientists and Engineers.

Jiang, T., Jiang, Y., Clark, D., Gray, R., and Brost, D. (2018). A compressive seismic field

trial and reconstruction test using regular indexing. pages 86–90. Society of Exploration Geophysicists.

Kimmel, R. and Sethian, J. A. (1996). Fast marching methods for computing distance maps shortest paths. Technical report, Lawrence Berkeley Nat. Lab., Berkeley, CA.

Kolda, T. G. and Bader, B. W. (2009). Tensor decompositions and applications. *SIAM Review*, 51:455–500.

Komatitsch, D. and Martin, R. (2007). An unsplit convolutional perfectly matched layer improved at grazing incidence for the seismic wave equation. *GEOPHYSICS*, 72(5):SM155–SM167.

Krizhevsky, A., Sutskever, I., and Hinton, G. E. (2017). Imagenet classification with deep convolutional neural networks. *Communications of the ACM*, 60:84–90.

Kumar, D. and Ahmed, I. (2011). *Seismic Noise*, pages 1157–1161. Springer Netherlands, Dordrecht.

Lathauwer, L. D., Moor, B. D., and Vandewalle, J. (2000). A multilinear singular value decomposition. *SIAM Journal on Matrix Analysis and Applications*, 21:1253–1278.

LeCun, Y., Bengio, Y., and Hinton, G. (2015). Deep learning. *Nature*, 521:436–444.

Liner, C. L. (2016). *Elements of 3D Seismology*. Society of Exploration Geophysicists.

Liu, Q., Fu, L., and Zhang, M. (2021). Deep-seismic-prior-based reconstruction of seismic data using convolutional neural networks. *Geophysics*, 86(2):V131–V142.

Liu, W., Cao, S., Li, G., and He, Y. (2015). Reconstruction of seismic data with missing traces based on local random sampling and curvelet transform. *Journal of Applied Geophysics*, 115:129–139.

Lopez, O., Kumar, R., Yilmaz, O., and Herrmann, F. J. (2016). Off-the-Grid Low-Rank Matrix Recovery and Seismic Data Reconstruction. *IEEE Journal of Selected Topics in Signal Processing*, 10(4):658–671.

Ma, J. (2013). Three-dimensional irregular seismic data reconstruction via low-rank matrix completion. *GEOPHYSICS*, 78(5):V181–V192.

Manohar, K., Brunton, B. W., Kutz, J. N., and Brunton, S. L. (2018). Data-driven sparse sensor placement for reconstruction: Demonstrating the benefits of exploiting known patterns. *IEEE Control Systems*, 38:63–86.

Monsegny, J. (2017). Bi-objective optimization for seismic survey design. pages 274–278. Society of Exploration Geophysicists.

Mosher, C. C., Keskula, E., Kaplan, S. T., Keys, R. G., Li, C., Ata, E. Z., Morley, L. C., Brewer, J. D., Janiszewski, F. D., Eick, P. M., Olson, R. A., and Sood, S. (2012). Compressive seismic imaging. pages 1–5. Society of Exploration Geophysicists.

Nadipally, M. (2019). *Optimization of methods for image-texture segmentation using ant colony optimization.* Elsevier Inc.

Pascanu, R., Mikolov, T., and Bengio, Y. (2013). On the difficulty of training recurrent neural networks. pages 1310–1318.

Popa, J., Minkoff, S. E., and Lou, Y. (2021). An improved seismic data completion algorithm using low-rank tensor optimization: Cost reduction and optimal data orientation. *GEOPHYSICS*, 86(3):V219–V232.

Regone, C., Stefani, J., Wang, P., Gerea, C., Gonzalez, G., and Oristaglio, M. (2017). Geologic model building in seam phase ii — land seismic challenges. *The Leading Edge*, 36:738–749.

Ronneberger, O., Fischer, P., and Brox, T. (2015). U-net: Convolutional networks for biomedical image segmentation. In Navab, N., Hornegger, J., Wells, W. M., and Frangi, A. F., editors, *Medical Image Computing and Computer-Assisted Intervention – MICCAI 2015*, pages 234–241, Cham. Springer International Publishing.

Shannon, C. (1949). Communication in the presence of noise. *Proceedings of the IRE*, 37(1):10–21.

Shu, G., Shi, T., Huang, L., Gao, Z., Lv, G., Di, Z., and Huo, S. (2020). Compressive seismic data acquisition in a desert area of western China: A case study. *The Leading Edge*, 39(5):340–344.

Stone, D. G. and Meeder, C. A. (1994). *Designing surveys in two and three dimensions*. Society of Exploration Geophysicists.

Stéphane, M. (2009). Chapter 1 - sparse representations. In Stéphane, M., editor, *A Wavelet Tour of Signal Processing (Third Edition)*, pages 1–31. Academic Press, Boston, third edition edition.

Tang, S., Ding, Y., Zhou, H.-W., and Zhou, H. (2022). Reconstruction of Sparsely Sampled Seismic Data via Residual U-Net. *IEEE Geoscience and Remote Sensing Letters*, 19:1–5.

Titova, A., Wakin, M. B., and Tura, A. (2019). Mutual coherence in compressive sensing seismic acquisition. pages 122–126. Society of Exploration Geophysicists.

Titova, A., Wakin, M. B., and Tura, A. (2021). Two-stage sampling – A novel approach for compressive sensing seismic acquisition. In *First International Meeting for Applied Geoscience and Energy Expanded Abstracts*, number 4, pages 110–114. Society of Exploration Geophysicists.

Trickett, S., Burroughs, L., Milton, A., Walton, L., and Dack, R. (2010). Rank-reduction-based trace interpolation. pages 3829–3833. Society of Exploration Geophysicists.

Velasquez-Espejo, A. J. (2012). 3d multicomponent seismic characterization of a clastic reservoir in the middle magdalena valley basin, colombia.

Versteeg, R. (1994). The marmousi experience: Velocity model determination on a synthetic complex data set. *The Leading Edge*, 13:927–936.

Villarreal, O., León-López, K., Espinosa, D., Agudelo, W., and Arguello, H. (2019). Seismic source reconstruction in an orthogonal geometry based on local and non-local information in the time slice domain. *Journal of Applied Geophysics*, 170:103846.

Villarreal, O. P., León, K., Espinosa, D., Agudelo, W., and Arguello, H. (2018). Compressive sensing seismic acquisition by using regular sampling in an orthogonal grid. *2017 IEEE 7th International Workshop on Computational Advances in Multi-Sensor Adaptive Processing, CAMSAP 2017*, 2017-Decem:1–5.

Wang, H., Tao, C., Chen, S., Wu, Z., Du, Y., Zhou, J., Qiu, L., Shen, H., Xu, W., and Liu, Y. (2019). High-precision seismic data reconstruction with multi-domain sparsity constraints based on curvelet and high-resolution Radon transforms. *Journal of Applied Geophysics*, 162:128–137.

Wang, S.-Q., Gao, X., and Yao, Z.-X. (2010). Accelerating pocs interpolation of 3d irregular seismic data with graphics processing units. *Computers & Geosciences*, 36:1292–1300.

Wang, Y., Cao, J., and Yang, C. (2011). Recovery of seismic wavefields based on compressive sensing by an l1-norm constrained trust region method and the piecewise random subsampling. *Geophysical Journal International*, 187:199–213.

Wang, Y., Wang, B., Tu, N., and Geng, J. (2020). Seismic trace interpolation for irregularly spatial sampled data using convolutional autoencoder. *GEOPHYSICS*, 85(2):V119–V130.

Wang, Z., Bovik, A., Sheikh, H., and Simoncelli, E. (2004). Image quality assessment: from

error visibility to structural similarity. *IEEE Transactions on Image Processing*, 13(4):600–612.

Wu, J., Bai, M., Zhang, D., Wang, H., Huang, G., and Chen, Y. (2020). Fast and robust low-rank approximation for five-dimensional seismic data reconstruction. *IEEE Access*, 8:175501–175512.

Yilmaz, O. (2008). *Seismic Data Analysis: Processing, Inversion, and Interpretation of Seismic Data*, volume 1. Society of Exploration Geophysicists.

Yin, P., Lyu, J., Zhang, S., Osher, S., Qi, Y., and Xin, J. (2019). Understanding Straight-Through Estimator in Training Activation Quantized Neural Nets. *7th International Conference on Learning Representations, ICLR 2019*, pages 1–30.

Yu, S. and Ma, J. (2021). Deep Learning for Geophysics: Current and Future Trends. *Reviews of Geophysics*, 59(3):1–36.

Zakaria, A. and Penrose, J. (2000). The Two Dimensional Numerical Modeling Of Acoustic Wave Propagation in Shallow Water. *... Conference (Acoustics)*, (November):1–6.

Zeiler, M. D. and Fergus, R. (2014). Visualizing and understanding convolutional networks.

Zhang, Y., Louboutin, M., Siahkoohi, A., Yin, Z., Kumar, R., and Herrmann, F. J. (2022). A simulation-free seismic survey design by maximizing the spectral gap. pages 15–20. Society of Exploration Geophysicists and American Association of Petroleum Geologists.